NUCLEAR SCIENCE AND ENGINEERING: **137**, 251–280 (2001)

Multiple Scattering in Clouds: Insights from Three-Dimensional Diffusion/P_1 Theory

Anthony B. Davis*

Los Alamos National Laboratory, Space and Remote Sensing Sciences Group (NIS-2)
Los Alamos, New Mexico 87545

and

Alexander Marshak

NASA's Goddard Space Flight Center, Climate and Radiation Branch (Code 913)
Greenbelt, Maryland 20771
and
Joint Center for Earth Systems Technology, University of Maryland - Baltimore County
Baltimore, Maryland 81250

Received January 18, 2000
Accepted August 18, 2000

Abstract—*In the atmosphere, multiple scattering matters nowhere more than in clouds, and being a product of its turbulence, clouds are highly variable environments. This challenges three-dimensional (3D) radiative transfer theory in a way that easily swamps any available computational resources. Fortunately, the far simpler diffusion (or P_1) theory becomes more accurate as the scattering intensifies, and allows for some analytical progress as well as computational efficiency. After surveying current approaches to 3D solar cloud-radiation problems from the diffusion standpoint, a general 3D result in steady-state diffusive transport is derived relating the variability-induced change in domain-average flux (i.e., diffuse transmittance) to the one-point covariance of internal fluctuations in particle density and in radiative flux. These flux variations follow specific spatial patterns in deliberately hydrodynamical language: radiative channeling. The P_1 theory proves even more powerful when the photon diffusion process unfolds in time as well as space. For slab geometry, characteristic times and lengths that describe normal and transverse transport phenomena are derived. This phenomenology is used to (a) explain persistent features in satellite images of dense stratocumulus as radiative channeling, (b) set limits on current cloud remote-sensing techniques, and (c) propose new ones both active and passive.*

I. MOTIVATION, CONTEXT, AND OVERVIEW

Low-altitude clouds (in the planetary boundary layer) are made of liquid water droplets in sizes and concentrations that make them highly reflective in much of the solar spectrum. In turn, this gives these clouds a critical role in balancing the Earth's radiative budget, so they have a first-order effect on climate and weather.[1] Unfortunately for numerical climate and weather modelers, clouds come in many shapes and forms. They are extremely complex structures not well understood in terms of their formation and life-cycle. They are not better understood from the standpoint of their basic optical properties, both at the macroscopic level that affects the radiation budget and at the microscale where turbulence prevails. Unresolved structure also makes the remote sensing of cloud properties a difficult task; even if the fine cloud structure is resolved by high-resolution imaging techniques, the three-dimensional (3D) radiative transfer it beckons cannot be applied operationally in the data processing. So the treatment of clouds in all aspects of atmospheric radiation science is a question of approximation, and determining the limitations of a given approximation is generally nontrivial.

High-altitude clouds (cirrus) are out of the scope of this study not because their optics are any simpler but

*E-mail: adavis@lanl.gov

because they are generally too thin optically to support diffusive radiation transport. The major source of complication in these clouds is that they are made of ice crystals that are not necessarily randomly oriented. So the single-scattering properties of cirrus are difficult to measure, to compute, and to incorporate into multiple scattering models.[2]

In the radiative transfer theorist's mind, *highly-reflective* automatically translates to *weakly absorbing and dominated by multiple scattering*, which, in turn, is an invitation to apply diffusion (or P_1) theory to the largest possible extent. This is conventional wisdom in neutron transport science and it will be our strategy here. A detailed survey of cloud radiation literature, even limited to 3D theory, would be overwhelming. However, a representative survey of prior applications of 3D photon diffusion theory in the geophysical literature is in order. In this community at least, it was fully realized that diffusion and P_1 theories were in fact equivalent until about the time Preisendorfer clarified this in his 1976 texts[3] in hydrological optics. So early papers, starting with Giovanelli[4] in 1959, systematically start with the general radiative transfer equation and rederive the formulas of photon diffusion before turning to an application. The problem of solar illumination, of particular interest here, has been worked out analytically for several 3D geometries. In plane-parallel geometry, the sine-wave cloud that we use extensively further on as an illustration was studied by perturbation analysis,[4,5] and exactly by eigenfunction analysis.[6] Several isolated cloud problems were similarly solved: homogeneous finite-height cylinders,[7] homogeneous rectangular parallelepipeds,[8] and full and hollow spheres.[9] Internal diffuse sources are also of interest in thermal infrared (IR) studies.[10] The trend is now to develop a general-purpose numerical code that implements a steady-state diffusion-based solution for an arbitrary distribution of scattering/absorbing material and both thermal and solar source terms.[11,12] Steady localized sources have also elicited some interest.[13] In most of these studies, diffusion theory is presented as a viable alternative to exact transport methods in perennial efficiency-versus-accuracy trade-off problems, and the solutions are generally validated against Monte Carlo or grid-based codes. The motivation behind almost all atmospheric radiation theories, photon diffusion included, is optical and/or thermal remote sensing (in which case radiances are sought) and climate (in which case fluxes are of primary interest). However, the lightning community has recently showed interest in time-dependent diffusion methods for localized sources,[14] a problem that is also of interest in cloud probing with lidar (light radar).[15]

The paper is organized as follows. In Sec. II, we introduce the required notations in radiative transfer with multiple scattering and survey the connections between this incarnation of linear transport theory and diffusion theory, including a recently uncovered one that makes no outright hypothesis on the radiance field. In Sec. III, we pose the general albedo problem in steady state using both radiative transfer and diffusion theories in a geometry suitable for atmospheric applications: collimated solar beam impinging from above onto a dense cloud layer. This problem is the focus of the next three sections, each introducing a successively better approach to its solution. Section IV uses the all-too-standard homogeneity assumption, thus neglecting all horizontal variability. In Sec. V we make use of the closed-form homogeneous solution but apply it locally. This independent pixel assumption is widely used in atmospheric radiation, although not necessarily at a scale where it works best; we explore its general predictions for large-scale averages and their consequences for climate. Section VI uses 3D diffusion theory to derive a general result that links the change in domain-averaged flux caused by the (arbitrary) variability to the cross-correlation between fluctuations in the extinction and local flux fields. This result illustrates the general mechanism by which radiation flow interacts with fluctuations in density that we call radiative channeling. Section VII is devoted to characteristic timescales and related length-scales of importance in diffusive transport through finite slab media, with and without absorption. In turn, these scales for diffusion are used in Sec. VIII to interpret some robust features observed in the spatial statistics of remotely sensed cloud radiance fields and, from there, to set bounds on the applicability of the independent-pixel approximation. In Sec. IX, we summarize our findings, describe some work-in-progress that uses 3D diffusion concepts, and we connect with stochastic radiative transfer (as it has been applied to problems in atmospheric radiation by G. C. Pomraning and friends).

II. RADIATIVE TRANSFER WITH MULTIPLE SCATTERING

In this section, we introduce notations for quantities of interest throughout this study and recall some basic results from radiative transfer and diffusion transport theories.

II.A. Radiative Transfer in 3+1 Dimensions

We seek the time-dependent radiance field $I(t, \boldsymbol{x}, \Omega) \geq 0$ as a function of propagation direction Ω on the unit sphere Ξ, at a point $\boldsymbol{x}$ in a domain M of $\mathcal{R}^3$, and at time t. We assume the (open) set M to be convex, meaning that exiting rays can not reenter the medium. This last assumption simplifies formulation but does not actually restrict the generality of our discussion because, at least up to the point where we take the diffusion limit, we can always set $\sigma(\boldsymbol{x}) = 0$ in some areas of M.

Inside the scattering/absorbing optical medium M, the radiance field is determined by[16,17]

1. The integrodifferential radiative transfer equation (RTE):

$$\left[c^{-1}\frac{\partial}{\partial \mathrm{t}} + \Omega\cdot\nabla\right] I$$

$$= -\sigma(\boldsymbol{x})I + \sigma_{\mathrm{s}}(\boldsymbol{x})\int p(\Omega\cdot\Omega')I(t,\boldsymbol{x},\Omega')\,d\Omega'$$

$$+ f(t,\boldsymbol{x},\Omega)\ , \qquad (1)$$

where the source term $f(t,\boldsymbol{x},\Omega)$ is specified.

2. Boundary conditions (BCs in the following) if $\mathrm{M} \neq \mathcal{R}^3$, specifically,

$$I(t,\boldsymbol{x},\Omega) \text{ is given, for all } t\ ,$$

where

$$\boldsymbol{x} \in \partial\mathrm{M} = \underline{\mathrm{M}}\backslash\mathrm{M}\ , \quad \text{and} \quad \Omega\cdot\boldsymbol{n}(\boldsymbol{x}) < 0\ ,$$

$\boldsymbol{n}(\boldsymbol{x})$ being outward normal to M's boundary ∂M at $\boldsymbol{x}$ ($\underline{\mathrm{M}}$ denotes the closure of M).

3. An initial condition if only $t \geq 0$ is of interest, specifically,

$$I(0,\boldsymbol{x},\Omega) \text{ is given for } \boldsymbol{x} \in \underline{\mathrm{M}}, \text{ and } \Omega \in \Xi\ .$$

Coefficients $\sigma(\boldsymbol{x})$ and $\sigma_{\mathrm{s}}(\boldsymbol{x})$ that appear in the RTE are given nonnegative fields describing the infinitesimal probabilities per unit of length of photon-matter interaction along an arbitrary beam, respectively, for extinction (either scattering or absorption) and for scattering alone. One more optical property needs to be specified: the scattering phase function, $p(\Omega\cdot\Omega')$, assumed in this study to depend only on the scattering angle $\theta_{\mathrm{s}} = \cos^{-1}(\Omega\cdot\Omega')$; we adopt the normalization convention, where

$$\int p(\Omega\cdot\Omega')\,\mathrm{d}\Omega = 1\ . \qquad (2)$$

Note that the aforementioned problem for photons is formally identical to (one-group) neutron transport, so apart from some points in terminology, much of this study carries over to nuclear science.

The key quantity in the RTE is the extinction field $\sigma(\boldsymbol{x})$ because it controls the photon free-path distribution, at the heart of the transport problem. Its inverse is the mean-free-path (mfp) only in one case, albeit a very well-studied one: $\sigma(\boldsymbol{x})$ is uniform in space; free paths are then exponentially distributed and thus entirely determined by the mfp, $\ell = 1/\sigma$. This restriction of the Bouger-Beer law of exponential extinction to strictly homogeneous situations is often overlooked. In heterogeneous media, the actual photon mfp depends nontrivially on the spatial correlations in $\sigma(\boldsymbol{x})$. Letting overscores designate spatial averages in the remainder of this paper, the actual value of ℓ can only occasionally be equal to $(\bar{\sigma})^{-1}$, the effective mfp in a homogeneous medium with the same average extinction. Under some circumstances, $\ell = \overline{1/\sigma}$, which is, in essence, the mean mfp. So extinction only determines a local mfp, the mfp the photons would have in a homogenous medium of equal opacity. The quantity that is still exponentially distributed (with unit mean) in 3D radiative transfer is

$$\tau(\boldsymbol{x},\Omega;s) = \int_0^s \sigma(\boldsymbol{x}+\Omega s')\,\mathrm{d}s'\ , \qquad (3)$$

the optical distance between $\boldsymbol{x}$ and $\boldsymbol{x}' = \boldsymbol{x} + \Omega s$, where $s = \|\boldsymbol{x}' - \boldsymbol{x}\|$ and $\Omega = (\boldsymbol{x}' - \boldsymbol{x})/s$.[a] Optical distance $\tau(\boldsymbol{x},\Omega;s)$ is a measure of the cumulative amount of scattering/absorbing material as s increases along the $(\boldsymbol{x},\Omega)$ beam, appropriately weighted by the photon-matter interaction cross section. For the famous exponential law to carry over to physical distance s (the photons' random free paths), we require proportionality between τ and s; i.e., $\sigma(\boldsymbol{x})$ is invariant in direction Ω starting at $\boldsymbol{x}$. If this is true for all $(\boldsymbol{x},\Omega)$, then $\sigma(\boldsymbol{x})$ is clearly uniform. Davis[9] gives a more powerful proof of this statement using characteristic-function theory in probability; moreover, he shows that 3D free-path distributions are always broader than exponential in the sense that $\langle s^2\rangle \geq 2\langle s\rangle^2 = 2\ell^2$; equivalently, the standard deviation of s exceeds its mean ℓ. Throughout this paper, angular brackets $\langle\cdot\rangle$ are used to denote ensemble averages, in this case, over photon trajectories.

An abundant source of challenging radiative transfer problems is the interaction of the Earth's cloudy atmosphere with solar and thermal photons, as well as radar and lidar beams. In this case, we can think of M either as the whole atmospheric column, $\mathrm{M} = \mathcal{R}^2 \otimes \mathcal{R}_+$ ($z \geq 0$ represents altitude), or a part of it, such as a cloud layer (between $z = z_{\mathrm{bot}} \geq 0$ and $z = z_{\mathrm{top}} \geq z_{\mathrm{bot}}$); either way, we neglect curvature effects, hence the infinite (x,y) extent of the column. Some optically relevant atmospheric constituents are primarily stratified, i.e., variable more in z than in x and y; examples are well-mixed absorbing trace gases (H_2O, CO_2, etc.) and scattering and absorbing aerosol particles. Others are highly variable in all three spatial directions, arguably more in the horizontal than in the vertical in some cases—cloud droplets for instance.

II.B. Scattering and Absorption

The extinction coefficient decomposes as follows, for scattering and for absorption:

$$\sigma(\boldsymbol{x}) = \sigma_{\mathrm{s}}(\boldsymbol{x}) + \sigma_{\mathrm{a}}(\boldsymbol{x})\ ; \qquad (4)$$

[a] This can be shown from Eq. (1) in steady state and without source terms: If $\ln I(\boldsymbol{x}',\Omega)|_{\boldsymbol{x}'=\boldsymbol{x}+\Omega s} = -\tau(\boldsymbol{x},\Omega;s) + \textit{constant}$, then we have $\Omega\cdot\nabla I \equiv \mathrm{d}I/\mathrm{d}s = -\sigma(\boldsymbol{x})I$, and conversely.

it is customary to define the relative probability of scattering as

$$\varpi_0 = \frac{\sigma_s(\boldsymbol{x})}{\sigma(\boldsymbol{x})} \leq 1 \ , \tag{5}$$

also known as the single-scattering albedo. As previously indicated, we require ϖ_0 to remain constant inside M for the remainder of the paper.

A quantity of particular interest in scattering media is the phase function's asymmetry factor:

$$g = \langle \mu_s \rangle = 2\pi \int_{-1}^{+1} \mu_s p(\mu_s)\, \mathrm{d}\mu_s \ , \tag{6}$$

where $\mu_s = \cos\theta_s$. This quantity is sufficient to specify the popular Henyey-Greenstein model[18]

$$p(\cos\theta_s) = \left(\frac{1}{4\pi}\right) \frac{1-g^2}{[1+g^2-2g\cos\theta_s]^{3/2}} \ , \tag{7}$$

used extensively in the following.

In many applications—particularly when multiply scattered photons dominate the bulk of the radiation field—simple phase functions such as Eq. (7) are adequate substitutes for more realistic ones, especially when one is only interested in fluxes as opposed to radiances. In dense boundary-layer clouds, a realistic phase function would be based on Mie scattering computations for spherical droplets followed by averaging over the observed droplet-size distributions.[19] This leads to $g \approx 0.85$ and justifies using the relation for asymptotically large particles with respect to wavelength: cross section (per particle) $\approx 2\pi r^2$. Thus σ (i.e., cross section $\times$ density) can easily be obtained from the effective droplet radius, $r_e = \langle r^3 \rangle / \langle r^2 \rangle$, and the meteorological quantity known as liquid water content (LWC) in grams per cubic metre: $\sigma = (2/3)\mathrm{LWC}/\rho_w r_e$, where ρ_w is the density of water 10^6 g/m^3. Typical values are $r_e \approx 8$ to 10 μm, LWC $\approx$ 0.7 g/m^3, hence $\sigma \approx 0.05$ m^{-1} (highly variable), which would correspond to $\ell \approx 20$ m in a homogeneous cloud.

II.C. Fluxes and Radiant Energy Conservation

In essence, Eqs. (2) and (6) characterize the zeroth- and first-order coefficients of the scattering phase function in a Legendre-polynomial expansion in $\cos\theta_s$. In the same way, we can project the radiance field $I(\cdot, \Omega)$ onto the space of isotropic functions on Ξ, with a nonnegative scalar coefficient

$$J(t, \boldsymbol{x}) = \int I(t, \boldsymbol{x}, \Omega)\, \mathrm{d}\Omega \tag{8}$$

on the one hand, and onto the orthogonal space of dipolar functions on Ξ, with a vector coefficient

$$\boldsymbol{F}(t, \boldsymbol{x}) = \int \Omega I(t, \boldsymbol{x}, \Omega)\, \mathrm{d}\Omega \tag{9}$$

on the other hand. This is equivalent to a spherical-harmonic (P_n) expansion to order 1. The quantity in Eq. (9) is the familiar (net) radiative flux vector field, whereas the quantity in Eq. (8) bears different names in different literatures: scalar flux,[3] spherical flux,[20] or actinic flux.[21] At any rate, it is related to the radiant energy (or photon) density field[17]

$$U(t, \boldsymbol{x}) = J(t, \boldsymbol{x})/c \ , \tag{10}$$

where c is the speed of light, or to mean radiance[16] $J(t, \boldsymbol{x})/4\pi$.

Integrating the RTE in Eq. (1) over Ξ and using Eqs. (2), (4), (5), (8), and (9), we obtain the expression of radiant energy (or photon number) conservation, with depletion and creation terms:

$$c^{-1} \frac{\partial}{\partial t} J + \nabla \cdot \boldsymbol{F} = -\sigma_a(\boldsymbol{x}) J(t, \boldsymbol{x}) + S(t, \boldsymbol{x}) \ , \tag{11}$$

where $S(t, \boldsymbol{x}) = \int f(t, \boldsymbol{x}, \Omega)\mathrm{d}\Omega$ describes internal sources from the standpoint of $J(t, \boldsymbol{x})$. Now, in nuclear reactor theory, neutron multiplication is the important source of particles. Being proportional to density $J(t, \boldsymbol{x})$, this source can be modeled by formally making $\sigma_a(\boldsymbol{x}) < 0$ in Eq. (11); equivalently, $\varpi_0 > 1$ in Eq. (5) is the multiplication factor. In that same context, scattering is often considered isotropic, $g \approx 0$ in Eq. (6).

If $\sigma_a(\boldsymbol{x}) = 0$ ($\varpi_0 = 1$) and, in the absence of internal sources, we see that the mean flow of the photon gas is irrotational in steady state, then

$$\nabla \cdot \boldsymbol{F} = 0 \ , \tag{12}$$

expressing local radiant energy conservation at all points in M. Geometrically, Eq. (12) means that radiative flux lines cannot form closed loops, neither can they start or end inside M, only at its boundary ∂M; several examples of such radiative flows are provided in the following pages.

II.D. Diffusion, as a Self-Consistent Transport Theory

We know of at least two roads from the RTE to diffusion theory, where it surfaces as a transport theory of interest in its own right:

1. invoking Fick's constitutive law to close the transport problem partially posed in Eqs. (11) or (12)
2. a formal limit in discrete-angle (DA) radiative transfer theory.

Fick's law relates $\boldsymbol{F}$ to $J = cU$ through

$$\boldsymbol{F}(t, \boldsymbol{x}) = -[D(\boldsymbol{x})/c] \nabla J \ , \tag{13}$$

where $D(\boldsymbol{x})$ is diffusivity, the fundamental quantity in diffusion theory. It is related to the photon's (local) transport mfp $\ell_t(\boldsymbol{x})$ as follows[22]:

$$D(\boldsymbol{x})/c = \ell_{\mathrm{t}}(\boldsymbol{x})/3 \ , \tag{14}$$

and, from there, to extinction in[b]

$$\ell_{\mathrm{t}}(\boldsymbol{x}) = 1/[(1-\varpi_0 g)\sigma(\boldsymbol{x})] \ , \tag{15}$$

where $\sigma(\boldsymbol{x})^{-1}$ is the local mfp and g is >0 for scattering preferentially in the forward direction. The transport mfp in Eq. (15) is probably the single most important length scale in diffusion theory.

In statistical physics, Eq. (13) is a constitutive law, which is always paired with a continuity equation, in this case Eq. (11) or (12), expressing particle-number conservation in the course of diffusive motion. Fick's law is intuitively appealing: photons flow from high to low photon concentrations at a rate proportional to $\ell_{\mathrm{t}}(\boldsymbol{x})$. There are many other continuity-constitutive equation pairs: charge conservation and Ohm's law, energy conservation and Fourier's law, fluid mass conservation and D'Arcy's law, etc. Photon diffusion theory thus inherits from a vast culture in the physical sciences.

Photon diffusion theory also inherits from the more mathematical culture of probability and statistics: We can think of the photons as particles in Brownian motion, i.e., following convoluted "drunkard's paths" made of a long sequence of short steps in random directions. In this framework of random walk theory, scattering with $g>0$ is equivalent to short-time directional correlations that cause persistent motion in the original direction of the beam.[23] Rescaling of mfp's by $(1-\varpi_0 g)^{-1} > 1$ in Eq. (15) accounts for the extent of this drift that cumulates over several scatterings, and $\ell_{\mathrm{t}}(\boldsymbol{x})$ can be interpreted as the effective mfp for a single-but-isotropic scattering.

Combining Eqs. (11) and (13), we find the parabolic partial differential equation (PDE)

$$c^{-1}\left[\frac{\partial}{\partial t} - \nabla\cdot D(\boldsymbol{x})\nabla + c\sigma_a(\boldsymbol{x})\right]J = S(t,\boldsymbol{x}) \ , \tag{16}$$

where we identify another characteristic scale,

$$\begin{aligned} L_{\mathrm{d}}(\boldsymbol{x}) &= \sqrt{\mathrm{D}(\boldsymbol{x})/c\sigma_{\mathrm{a}}(\boldsymbol{x})} \\ &= \sigma(\boldsymbol{x})^{-1}[3(1-\varpi_0)(1-\varpi_0 g)]^{-1/2} \ , \end{aligned} \tag{17}$$

known as the (local) diffusion length. In a homogeneous medium, the physical meaning of L_{d} is that a significant number of photons will have been destroyed by absorption at this distance from their source. The analog of L_{d} in nuclear reactor theory ($\varpi_0 > 1$, $g \approx 0$) is the size factor, $\ell_{\mathrm{t}}/(\varpi_0 - 1)^{1/2}$, that determines the critical mass in a given geometry.

For future reference, we define the spatially invariant ratios

$$\kappa(\varpi_0, g) = \frac{1}{\sigma(\boldsymbol{x})L_{\mathrm{d}}(\boldsymbol{x})} = \sqrt{3(1-\varpi_0)(1-\varpi_0 g)} \tag{18}$$

and

$$\xi(\varpi_0, g) = \frac{\ell_{\mathrm{t}}(\boldsymbol{x})}{L_{\mathrm{d}}(\boldsymbol{x})} = \sqrt{\frac{3(1-\varpi_0)}{1-\varpi_0 g}} \ , \tag{19}$$

sometimes called the similarity factor.[24]

The alternative connection between diffusion and DA radiative transfer theories is a relatively recent finding by Lovejoy et al.[25] DA radiative transfer theory follows from the RTE in Eq. (1) with a special choice of phase function made of a discrete sum of Dirac δ functions on Ξ; the requirement of phase function dependence only on $\Omega\cdot\Omega'$ limits the δ's to the vertices of regular polyhedra. The most popular case uses the sixfold symmetry of the octahedron (dual surface of the cube) that lines up with the orthogonal Cartesian axis: DA photons can scatter forward ($\theta_{\mathrm{s}} = 0$), backward ($\theta_{\mathrm{s}} = \pi$), or sideways ($\theta_{\mathrm{s}} = \pi/2$, with four different azimuthal possibilities, $\varphi_{\mathrm{s}} = 0$, $\pi/2$, π, and $3\pi/2$), and the respective probabilities of these events add up to unity. By the same token, the new RTE is not an integrodifferential equation but a discrete system of six coupled PDEs for the six fluxes of photons propagating in $\pm x$, $\pm y$, and $\pm z$ directions, where the phase function integral is replaced by a 6×6 scattering matrix. By formally manipulating the phase-function parameters in a representation that diagonalizes the scattering matrix, one can emphasize side-scattering to the point where some of the phase-function parameters take nonphysical (negative) values in their natural representation; at the same time however, the PDE system collapses onto a scalar diffusion equation and a Fickian vector relation. This approach to diffusion is novel in that it makes no outright assumptions on the radiance like most other approaches; only phase functions are changed. It also presents the standard (RTE-based) theory, DA theory, and diffusion theory in a unified formalism where each photon-transport theory has a distinctive mathematical character, rather than just a hierarchy of approximations.

II.E. Diffusion, as an Approximation to Radiative Transfer

There are also well-traveled roads from the RTE to diffusion theory that present it as an approximation to the more general linear transport theory encapsulated in the RTE:

[b] We quote here the standard result from transport theory and defer our discussion of the currently debated dependence of D on ϖ_0 until Sec. II.E.

1. P_1 truncation,[22] i.e., at first order in the spherical-harmonic expansion of the RTE
2. asymptotic theory.[26]

From this standpoint, we represent—when and where possible—the radiance field $I(t, \boldsymbol{x}, \Omega)$ with the scalar and vector quantities $J(t, \boldsymbol{x})$ and $\boldsymbol{F}(t, \boldsymbol{x})$; we therefore have

$$I(t, \boldsymbol{x}, \Omega) \approx [J(t, \boldsymbol{x}) + 3\Omega \cdot \boldsymbol{F}(t, \boldsymbol{x})]/4\pi \ , \qquad (20)$$

as can be verified directly by substitution into Eqs. (8) and (9). In other words, $I(t, \boldsymbol{x}, \Omega)$ is presumably well-approximated on Ξ by the sum of an isotropic term and a dipole term. Using Fick's law [Eq. (13)] with Eqs. (10) and (14), we can eliminate the flux field from Eq. (20):

$$I(t, \boldsymbol{x}, \Omega) \approx [1 - \ell_t(\boldsymbol{x})\Omega \cdot \nabla] J(t, \boldsymbol{x})/4\pi \ . \qquad (21)$$

When and where is this likely to be a reasonable representation? The short answer is: not too close to photon sources, especially if they are directional and/or localized and/or rapidly evolving; not too close to sinks either. This has ramifications in space and time as well as for the scattering and absorption properties of the optical medium. We now visit each item individually.

1. In space, sources can be internal or at boundaries. Internal ones are often thermal, hence isotropic, which is good for diffusion. In contrast, boundary sources are often collimated and sometimes localized too, which is bad for diffusion. More bad news for diffusion: Boundaries are generally radiation sinks and often sources as well, depending on direction of propagation Ω. However, a high-reflectance Lambertian (isotropic) boundary is good news. There is a way of stating this requirement quantitatively, at least of conservative ($\varpi_0 = 1$) systems. We let H denote the smallest of M's outer dimensions, which is then the only other length scale of any immediate consequence beyond the (local) mfp $\ell(\boldsymbol{x}) = 1/\sigma(\boldsymbol{x})$; we therefore require

$$H/\ell(\boldsymbol{x}) = \sigma(\boldsymbol{x})H \gtrsim 1 \qquad (22)$$

for photon diffusion to occur. A reasonable cut-off value for $\gtrsim$ is[27] 1 to 2 times $(1 - g)^{-1}$. It is not clear, however, whether $(1 - g)\sigma(\boldsymbol{x})H = H/\ell_t(\boldsymbol{x})$ needs to exceed unity everywhere or only most of the time in variable media such as clouds. At any rate, the larger is the ratio in Eq. (22), which we can interpret as the optical distance through the smallest chord of M, the higher is the prevailing order-of-scattering; this is intuitive, but we will restate this quantitatively in Sec. VII. In turn, many scatterings (less memory of direction to sources) will make Eq. (20) a reasonable representation of $I(t, \boldsymbol{x}, \Omega)$. This makes the absorbing boundaries opposite those boundaries with sources in optically thick media (e.g., the bases of dense clouds in daylight) look like a good place for diffusion; unfortunately, diffusion is disrupted near such boundaries too because many of the photons that have arrived there after many scatterings can now escape by collective streaming motion (i.e., higher-order harmonics are excited). In summary, there is a boundary layer of thickness $\approx \ell_t(\boldsymbol{x})$, $\boldsymbol{x} \in \partial$M, where photon transport necessarily is nondiffusive.

2. Concerning temporal behavior, a cursory comparison of the RTE in Eq. (1) and the diffusion equation in Eq. (16) reveals that the RTE is relativistically invariant, but its diffusion counterpart is not. Solutions of the diffusion equation for a pulsed source (temporal Green functions) have the equivalent of radiative shocks—unphysical infinite velocities—at early times. Again, this is because the photons are still primarily in streaming motion near the source. One needs to wait a few times scales associated with the transport mfp to see the accuracy of the diffusion approximation improve:

$$t \gtrsim \ell_t(\boldsymbol{x})/c = 3D(\boldsymbol{x})/c^2 \ . \qquad (23)$$

3. Concerning scattering, it is clear that a phase function that varies over almost five orders of magnitude (half of which are within a degree or so of $\theta_s = 0$) is detrimental to diffusion theory. Unfortunately, this is precisely the case in typical cloud environments due to the diffraction peak.[19]

4. Concerning absorption, it is clear that the larger is $\sigma_a = (1 - \varpi_0)\sigma$, the lesser is the number of scatterings for the photon population at large. For a sufficient number of scatterings to occur without prior absorption so that Eq. (20) becomes reasonably accurate, we need to have $\ell_t \gtrsim L_d$. Using the definition in Eq. (19), this translates to $\xi(\varpi_0, g) \gtrsim 1$; hence,

$$\varpi_0 \gtrsim \frac{2}{3 - g} \ , \qquad (24)$$

which is the critical single-scattering albedo for a given asymmetry factor. For most atmospheric applications $g \approx 0.75$ to 0.85, so we find that ϖ_0 should exceed 0.89 to 0.93.

The next question is of course: Are there fixes for these shortcomings of diffusion theory?

1. In space, we are dealing with a typical boundary-layer problem where the diffusive solution applies in the bulk of the medium and a photon-streaming solution applies close to the boundaries. An approach based on short characteristics,[28,29] currently used to accelerate numerical radiative transfer, may be applicable in diffusion methods.

2. A first improvement on the early-time problem is to use the telegrapher's equation[30] with both first- and second-order derivatives in t instead of the standard parabolic PDE in Eq. (16); this results from having a time derivative of $F(t, \boldsymbol{x})$ in Eq. (13), as is normally required by a first-order harmonic (P_1) truncation of the RTE. Pomraning and others devoted much effort into improving the performance of diffusion theory near sources and boundaries and in optically thin regions, especially when

the fluxes vary rapidly in time (a common occurrence in neutron transport applications). The most powerful ideas were those of "variable Eddington factors" and "flux-limited" diffusion.[31,32]

3. If the goal of using diffusion is to have at hand a numerically efficient photon transport theory, and diffusion/P_1 theory does that, then its breakdown due to absorption is not too serious because the convergence rates of numerical RTE solvers generally increase with the relative amount of absorption. If the goal is to have at hand an analytically tractable theory, then the problem remains. In fact, challenging observational paradoxes have risen recently[33] following a controversial prediction by Furutsu and Yamada[34] that one should always use $\varpi_0 = 1$ in Eqs. (14) and (15) to obtain D. Rewriting Eqs. (14) and (15) as $c/D = 3\sigma[(1-g)\varpi_0 + \alpha(1-\varpi_0)]$, we have $\alpha = 1$ for the standard prediction (used in the following) and $\alpha = 0$ for the alternative prediction in diffusion theory, while the more accurate telegrapher's equation suggests[30] $\alpha = 1/3$. A fruitful approach here seems to be a careful application of asymptotic transport theory advocated by Aronson and Corngold.[35] These last authors arrive at $\alpha \approx 1 - (4/5)/(1+g)$ for Henyey-Greenstein scattering; for atmospheric particles with $g \approx 0.75$ to 0.85, we find intermediate values $\alpha \approx 0.54$ to 0.57.

4. With respect to scattering phase functions with strong diffraction peaks in the forward direction, there is a standard fix,[36] where the peak is modeled as a δ function at $\theta_s = 0$ with a weight $f > 0$: $p(\mu_s) = f\delta(1-\mu_s) + (1-f)[1+3g'\mu_s]$, where $g' = (g-f)/(1-f) < g$; the popular choice for f is g^2. Consequently, other optical properties are also rescaled: $\varpi_0' = \varpi_0(1-f)/(1-\varpi_0 f) \geq \varpi_0$ (= being for $\varpi_0 = 1$), and $\sigma'(\boldsymbol{x}) = (1-\varpi_0 f)\sigma(\boldsymbol{x}) < \sigma(\boldsymbol{x})$. These mappings leave invariant the coefficients on the left side of the diffusion equation in Eq. (16), but the source term on the right side is more distributed throughout the medium when used to represent the solar beam (as described in Sec. III); this improves the performance of the diffusion model.

The most important question is probably: How relevant is photon diffusion theory to atmospheric radiation transport? King, Radke, and Hobbs[37] measured radiance distributions inside marine stratocumulus, which are horizontally extended and unusually persistent cloud systems, hence climatically important. The authors frequently found angular signatures that can be accurately modeled by Eq. (20). An enumeration of less direct, but equally compelling, pieces of evidence that radiative transfer is primarily diffusive in dense boundary-layer clouds at large, is provided in Refs. 15 and 38. The reasonable success of asymptotic theory in cloud remote-sensing activity[39] at moderate resolution ($\approx$1 km) also bears witness to that fact.

III. THE GENERAL STEADY-STATE ALBEDO PROBLEM

In this section, we focus on albedo problems, implying a uniform and constant source located at the part of the boundary of M that is exposed to a collimated beam. After that, we return to time dependence and/or nonuniform sources.

III.A. Boundary Conditions and Responses in Radiative Transfer Theory

We seek the response $I(\boldsymbol{x},\Omega)$ in $\mathrm{M} \otimes \Xi$ to a steady and uniform external irradiation from a collimated (i.e., distant) source in some direction Ω_0 (photons travel in direction $-\Omega_0$):

$$I(\boldsymbol{x},\Omega) = \begin{cases} F_0\,\delta(\Omega+\Omega_0)\ , \\ \qquad \boldsymbol{x} \in \partial\mathrm{M}_{\mathrm{src}} = \{\boldsymbol{x} \in \partial\mathrm{M}; \boldsymbol{n}(\boldsymbol{x})\cdot\Omega_0 > 0\} \\ 0\ ,\ \ \boldsymbol{x} \in \partial\mathrm{M}_{\mathrm{snk}} = \partial\mathrm{M}/\partial\mathrm{M}_{\mathrm{src}} \end{cases} \tag{25}$$

and no internal source term in Eq. (1). Alternatively, this boundary source can be recast as an internal source for the diffuse component of the radiance field, which obeys homogeneous BCs; the source term in the RTE would then be $S_0(\boldsymbol{x},\Omega) = \varpi_0\sigma(\boldsymbol{x})F_0\exp[-\tau(\boldsymbol{x}_0,\boldsymbol{x})]p(-\Omega_0\cdot\Omega)$ where $\boldsymbol{x}_0(\boldsymbol{x},\Omega_0)$ is the piercing point with $\partial\mathrm{M}_{\mathrm{src}}$ of the beam going through $\boldsymbol{x}$ in direction Ω_0. In atmospheric work, F_0 is called the solar constant. The choice of subscripts refers to the presence of photon sources on one (connected) part of the convex boundary and photon sinks on the other part.

For specificity, consider a geometrically plane-parallel medium, i.e.,

$$\mathrm{M} = \{\boldsymbol{x} = (x,y,z)^{\mathrm{T}} \in \mathcal{R}^3;\ 0 < z < H\}\ , \tag{26}$$

where superscript T means transpose. We have $\Omega = (\sin\theta\cos\varphi, \sin\theta\sin\varphi, \cos\theta)^{\mathrm{T}}$, where it is customary to denote the z component of Ω by $\mu = \cos\theta$. Note that this simple external geometry does not exclude arbitrary internal variability. For instance, in Fig. 1a, we show a plane-parallel optical medium with

$$\begin{cases} \sigma(\boldsymbol{x}) \equiv \sigma(x) = \bar{\sigma} + \delta\sigma(x) \\ \delta\sigma(x) = -\delta\sigma_{\max}\cos(2\pi x/L) \end{cases}\ , \tag{27}$$

where L is the period of the extinction oscillation, independently of y and z, and we require $\delta\sigma_{\max} \leq \bar{\sigma}$ to keep the field nonnegative. This simple sine-wave cloud model will be used extensively in the following sections to illustrate three different approaches to 3D radiation transport problems.

In atmospheric applications, Eq. (26) is used to describe a stratiform cloud layer; in this context, z is

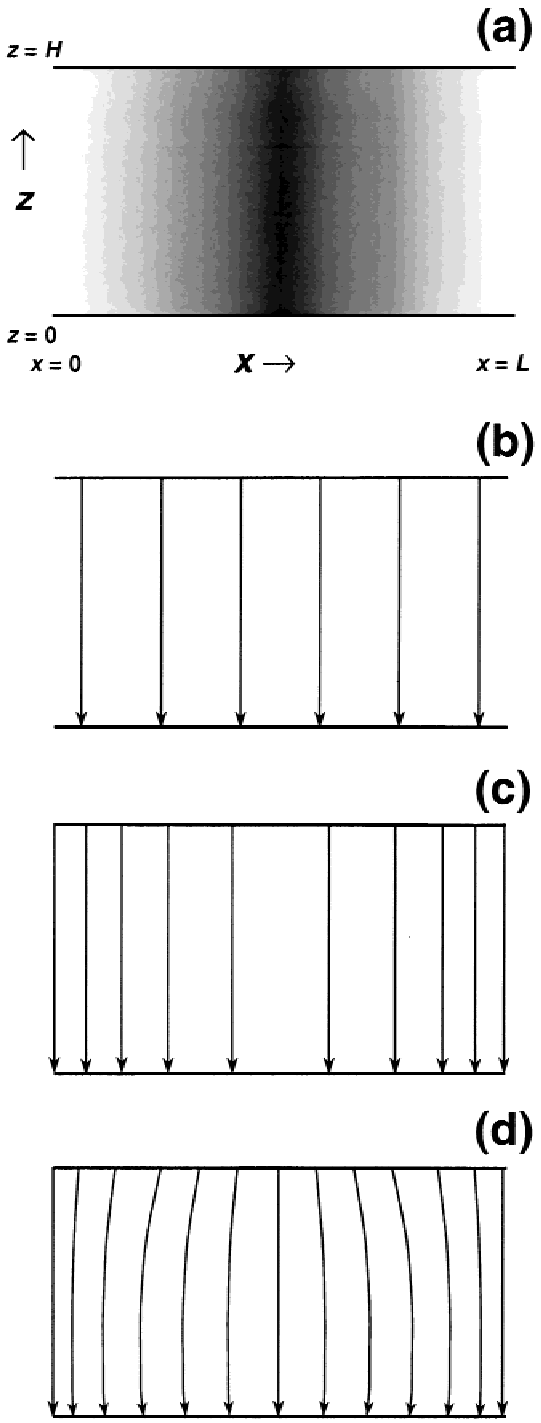

Fig. 1. Simple model of an internally variable, purely scattering optical medium illuminated uniformly from above, and three approaches for the radiation transport therein. (a) We take extinction from Eq. (27) and $\tau(x) = \sigma(x)H$ for optical depth where necessary. So there is a single variability scale, period L of the sine wave, to which a well-defined amplitude is assigned, $\delta\sigma_{\max} \leq \bar{\sigma}$. Schematics for three different solutions to this problem are illustrated in the other panels. (b) Flux lines in HPP theory as it is generally applied to horizontally variable clouds by using the mean extinction. (c) Flux lines in the IPA. (d) Flux lines in 3D transport theory, described with 3D diffusion.

assigned to the vertical. We can therefore set $\Omega_0 = ([1-\mu_0^2]^{1/2}, 0, \mu_0)^{\mathrm{T}}$, $0 < \mu_0 \leq 1$ describing collimated (i.e., solar) illumination from above at an angle $\theta_0 = \cos^{-1}\mu_0$ from zenith in a principal plane defined by $\varphi = \varphi_0 = 0$ (constant y). This natural convention leads to

$$\partial\mathrm{M} = \partial\mathrm{M}_{\mathrm{src}} \cup \partial\mathrm{M}_{\mathrm{snk}} \begin{cases} \partial\mathrm{M}_{\mathrm{src}} = \{\boldsymbol{x} \in \mathcal{R}^3\ z = H\} \\ \partial\mathrm{M}_{\mathrm{snk}} = \{\boldsymbol{x} \in \mathcal{R}^3;\ z = 0\} \end{cases} . \quad (28)$$

In many cases, we are interested in the unknown radiance fields at the boundaries: the escaping (hence remotely observable) radiance fields, not given by the BCs but by the solution of the RTE. More precisely, we seek $I(x,y,H,\Omega)$ for $\boldsymbol{n}(x,y,H)\cdot\Omega(\mu,\varphi) = \mu \geq 0$ and $I(x,y,0,\Omega)$ for $\boldsymbol{n}(x,y,0)\cdot\Omega(\mu,\varphi) = -\mu \geq 0$. The former contributes to local reflectance (or albedo), namely,

$$R(x,y) = \frac{1}{\mu_0 F_0}\int_{\mu\geq 0} \mu I(x,y,H,\mu,\varphi)\,\mathrm{d}\mu\mathrm{d}\varphi \ , \quad (29a)$$

and the latter, to local transmittance,

$$T(x,y) = \frac{1}{\mu_0 F_0}\int_{\mu\leq 0} |\mu| I(x,y,0,\mu,\varphi)\,\mathrm{d}\mu\mathrm{d}\varphi \ , \quad (29b)$$

where

$$\mu_0 F_0 = \int_{\mu<0} |\mu| I(x,y,H,\mu,\varphi)\,\mathrm{d}\mu\mathrm{d}\varphi \quad (30)$$

is the uniform incoming flux, normal to the upper boundary, according to Eqs. (25) and (28). Note that these quantities are all hemispherical (rather than net) vertical fluxes.

There is a variety of general-purpose publicly available numerical transport codes that can compute the boundary fields in Eqs. (29a) and (29b) as well as internal fields. Packages such as DANTSYS (Ref. 40), originally designed for neutron transport, can be adapted to atmospheric geometries and optics. Currently, the popular choice in the cloud-radiation community is Evans's SHDOM model.[41] For a comprehensive survey, we refer the reader to the ongoing Intercomparison of 3D Radiation Codes (I3RC) Web site ⟨http://climate.gsfc.nasa.gov/I3RC⟩ for details on and performance of each model.

III.B. Boundary Conditions and Responses in Diffusion Theory

In the P_1 framework, the only available quantities are $J(\boldsymbol{x})$ and $\boldsymbol{F}(\boldsymbol{x})$, as related by Fick's law. It is customary to write the BCs for the PDE in Eq. (16) as

$$\begin{cases} \frac{1}{2}\left[1 + \chi\ell_{\mathrm{t}}(\boldsymbol{x})\frac{\partial}{\partial z}\right] J(\boldsymbol{x}) = \mu_0 F_0 \ , & \boldsymbol{x} \in \partial\mathrm{M}_{\mathrm{src}} \\ \frac{1}{2}\left[1 - \chi\ell_{\mathrm{t}}(\boldsymbol{x})\frac{\partial}{\partial z}\right] J(\boldsymbol{x}) = 0 \ , & \boldsymbol{x} \in \partial\mathrm{M}_{\mathrm{snk}} \end{cases} , \quad (31)$$

where $\chi\ell_t(\boldsymbol{x})$ is the extrapolation length at some $\boldsymbol{x} \in \partial M$, and the numerical constant χ is essentially a free parameter used to make diffusion a better approximation to the RTE in some respect. From Eq. (31), we note that J does not vanish at the lower boundary but, at a distance $J/|\partial_z J| = \chi\ell_t$ below it, J linearly extrapolates to zero. Here again, one can use homogeneous BCs on ∂M_{src} as well as ∂M_{snk} when $J(\boldsymbol{x})$ represents only the diffuse radiance field; in this case, an internal source term is required in Eq. (16) to model the deposition of solar photons in the medium: $S_0(\boldsymbol{x}) = \varpi_0\sigma(\boldsymbol{x})F_0 \exp[-\tau(\boldsymbol{x}_0(\boldsymbol{x}, \Omega_0), \boldsymbol{x})]$.

There is no unique method for determining χ from previously defined parameters in the problem. To wit, we have

$$\chi = \begin{cases} \text{one-third, from Fick's law and Eq. (20)} \\ \text{two-thirds, in Eddington's approximation} \\ 0.7104\ldots, \text{ from Milne's problem} \\ \text{four-thirds, in the optically thin limit} \end{cases} . \tag{32}$$

It was soon realized that Fick's law, and thus diffusion altogether, fails near cloud boundaries as photon trajectories become more ballistic and less like random walks. Milne's problem (a semi-infinite medium with isotropically scattering and uniform internal sources) was used extensively as a benchmark for diffusion theory. Notice how Eddington[42] arrived at a value quite close to the exact one.

In analogy with Eq. (31) for the incoming fluxes, the unknown flux fields describing the radiation that eventually escapes the medium in Eqs. (18a) and (18b) are, respectively,

$$R(x,y) = \frac{1}{2\mu_0 F_0}\left[1 - \chi\ell_t(x,y)\,\frac{\partial}{\partial z}\right] J(x,y,z)|_{z=H} \tag{33a}$$

and

$$T(x,y) = \frac{1}{2\mu_0 F_0}\left[1 + \chi\ell_t(x,y)\,\frac{\partial}{\partial z}\right] J(x,y,z)|_{z=0} \tag{33b}$$

after normalization by $\mu_0 F_0$. Combining with Eq. (31), we find

$$R(x,y) = J(x,y,H)/\mu_0 F_0 - 1 \tag{34a}$$

and

$$T(x,y) = J(x,y,0)/\mu_0 F_0 \ . \tag{34b}$$

In transport theory, $R(\cdot)$ and $T(\cdot)$ in Eqs. (29a) and (29b) are simple ratios of radiative fluxes. In diffusion theory, this is no longer true as soon as $\chi \neq 1/3$ in Eq. (32) because the assumed relation between J and flux (Fick's law) does not apply near the boundaries. However, it is natural to want to estimate net radiative fluxes inside the medium from $R(\cdot)$ and $T(\cdot)$. For instance, in the absence of absorption, the spatial integrals R and T of $R(x,y)$ and $T(x,y)$, respectively, add up to unity, and T is the mean flux through the cloud divided by $\mu_0 F_0$; by energy conservation, $\mu_0 F_0 T$ should be the result of integrating $\boldsymbol{n}(\boldsymbol{x})\cdot\boldsymbol{F}(\boldsymbol{x})$ over any surface inside M that covers its boundary (i.e., has the same extent in x, y). Using Fick's law and the lower BC in Eq. (31), we find however from Eq. (34b) that the mean value of F_z over the boundary domain is $\mu_0 F_0 T/3\chi$.

III.C. Bulk Radiative Energy Budget

We now examine radiant energy conservation within a finite volume. Consider the rectangular parallelepiped,

$$C(r;x,y) = \{(x',y',z')^{\mathrm{T}} \in \mathcal{R}^3;\, x < x' < x + r,\; y < y' < y + r,\, 0 \le z' \le H\} \ , \tag{35}$$

noting that the choice of a square (rather than a circle) for the horizontal cross section of this cylinder is not important for the following but simplifies formulas. Now integrate Eq. (11) with $\partial J/\partial t \equiv 0$ over all points in $C(r;x,y)$. Using the divergence theorem to replace the volume integral by a surface integral on the left side and dividing both sides by the total incoming radiation (namely, $r^2\mu_0 F_0$), we obtain

$$[\bar{R}(r;x,y) - 1] + [\bar{T}(r;x,y) - 0] + \bar{\Delta}(r;x,y) = -\bar{A}(r;x,y) \ , \tag{36}$$

where

1. the first term [in square brackets] comes from the net flux through $\partial M_{src} \cap C(r;x,y)$, with

$$\bar{R}(r;x,y) = \frac{1}{r^2}\int_x^{x+r}\int_y^{y+r} R(x',y')\,\mathrm{d}y'\mathrm{d}x' \ , \tag{37a}$$

   where $R(x,y)$ is obtained from Eq. (29a) or Eq. (33a), depending on whether the RTE or the diffusion equation is used to model the transport process

2. same remark for the second term, but through $\partial M_{snk} \cap C(r;x,y)$ this time, so

$$\bar{T}(r;x,y) = \frac{1}{r^2}\int_x^{x+r}\int_y^{y+r} T(x',y')\,\mathrm{d}y'\mathrm{d}x' \ , \tag{37b}$$

   where the integrand is obtained from Eq. (29b) or Eq. (33b)

3. the third term is the net flux through $M \cap \partial C(r;x,y)$, expressed in units of $r^2\mu_0 F_0$ spelled out in Eq. (39)

4. finally, on the right side, we have bulk absorptance

$$\bar{A}(r;x,y) = \frac{1}{r^2\mu_0 F_0}\int_0^H\int_y^{y+r}\int_x^{x+r}\sigma_a(x',y',z)J(x',y',z)\,dx'dy'dz \ . \tag{37c}$$

Rearranging the terms in Eq. (36) for easier interpretation, we have[43]

$$\bar{R}(r;x,y) + \bar{T}(r;x,y) + \bar{A}(r;x,y) = 1 - \bar{\Delta}(r;x,y) \ , \tag{38}$$

where the only inherently 3D term is

$$\bar{\Delta}(r;x,y) = \frac{1}{r^2\mu_0 F_0}\int_0^H\left\{\int_y^{y+r}[+F_x(x+r,y',z) - F_x(x,y',z)]\,dy' + \int_x^{x+r}[+F_y(x',y+r,z) - F_y(x',y,z)]\,dx'\right\}dz \ , \tag{39}$$

with F_x and F_y denoting net fluxes in the x and y directions, respectively. It accounts for losses and gains through the sides of the column, i.e., photons that are not reflected, transmitted, or absorbed within the confines of $C(r;x,y)$. There is at least one sure case where the 3D term $\bar{\Delta}(r;x,y)$ vanishes identically (for all x,y): Take $r = L$, the size of the computational domain in a numerical simulation with cyclical BCs in the horizontal.

In the energy balance equation (38) of a cloud, or the whole atmosphere, only $\bar{R}(r;\cdot)$ and $\bar{T}(r;\cdot)$ can be estimated from data using radiometers above and below the system. It is clearly important to find the scale r at which the contribution of $\bar{\Delta}(r;\cdot)$ to the radiation budget can justifiably be neglected. This has been done, at least for dense stratiform clouds like marine stratocumulus,[38,43] as explained in Sec. VIII. Another approach that in principle can work at very small scales is to somehow remove the effect of horizontal fluxes empirically. With this in mind, Ackerman and Cox[44] obtained the apparent absorption $\bar{\Delta}(r;\cdot) = 1 - [\bar{R}(r;\cdot) + \bar{T}(r;\cdot)]$ at visible wavelengths, where $\bar{A}(r;\cdot) \equiv 0$, and, assuming its counterpart in the near IR spectrum is comparable in magnitude and sign, then derived a less-biased estimate of $\bar{A}(r;\cdot)$. An improved version of this technique is described by Marshak et al.[45]

IV. ZEROTH-ORDER SOLUTION: HOMOGENEOUS PLANE-PARALLEL THEORY

IV.A. Enforced Global Translational Symmetry (Ignoring Horizontal Variability)

Within the framework of plane-parallel geometry, Eq. (26), we now assume

$$\sigma(\boldsymbol{x}) \equiv \sigma(z) \ . \tag{40}$$

In the absence of horizontal fluxes driven by nonuniform illumination, we then have

$$\frac{\partial}{\partial x}, \frac{\partial}{\partial y} \equiv 0 \tag{41}$$

in the Eq. (1) RTE and Eqs. (11) or (12) and (13) for diffusion. This defines the horizontally homogeneous plane-parallel (HPP) problem, a standard in many applications, including atmospheric science: HPP theory is still used operationally in many situations, remote sensing and climate forecasting in particular.

We view HPP theory as a reference with which to compare "better" theory for a horizontally variable medium. Presumably, $\sigma(z)$ in Eq. (40) is identified with the average value of $\sigma(x,y,z)$ over a given z plane; this is a natural choice because σ is proportional to particle density, and $\sigma(z)$ would be predicated on the mean density at level z. With respect to the general albedo problem, standard HPP theory is based on a voluntary neglect of horizontal variability. Effectively, we have imposed a strong degree of translational symmetry on the system.

Using Eq. (41) with Eq. (5), the RTE becomes

$$\mu\frac{dI}{d\tau_z} = -\left[I - \varpi_0\int p(\Omega\cdot\Omega')I(\tau_z,\Omega')\,d\Omega'\right] \tag{42}$$

in HPP theory, where we have set $d\tau_z = \sigma(z)dz$; Lenoble[20] extensively surveys solution methods. Furthermore, we take $\tau_0 = 0$ and

$$\tau = \int_0^H \sigma(z)\,dz = \tau_H \tag{43}$$

is the only parameter of interest: the (nondimensional) optical thickness of the slab. Recall that $1/\sigma$ is the photon mfp. So, if it is uniform in z, then $\tau = \sigma H$ is the slab's thickness in mfp's. In dense but nonprecipitating clouds, τ is highly variable at all scales, even when H is almost constant (e.g., marine stratocumulus). However, a typical value is 15. Using the cloud microphysical parameters quoted earlier, this translates to $\approx 0.2\ kg/m^2$ of liquid cumulated in the droplets and, in turn, this amounts to only ≈ 0.2 mm of water. There is generally approximately two orders of magnitude more water vapor in the column.

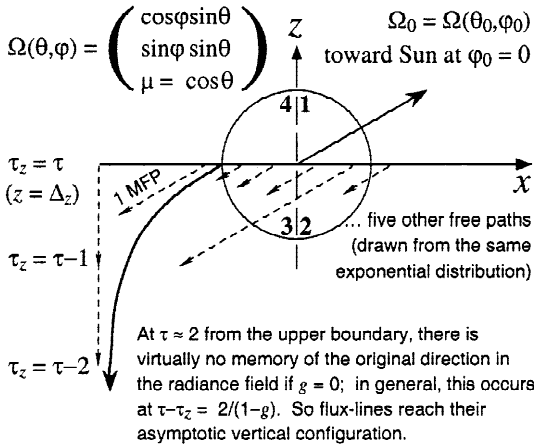

Fig. 2. Computation of net horizontal flux at upper boundary under slant illumination. Four quadrants are defined to give meaning to Eq. (31). Quadrants 2 and 3 make up the inward hemisphere, where radiance $I(\boldsymbol{x},\Omega)$ is specified by the boundary conditions. In the other two quadrants, we find the angular distribution of escaping radiance ($\Omega_z \geq 0$), as determined by the radiative transfer equation. We have drawn a typical flux line in the prediffusive domain ($0 < \tau_z \lesssim 2/(1-g)$ according to van de Hulst,[27]) assuming for simplicity azimuthal symmetry in the albedo field.

If the BCs are axisymmetric, i.e., $\Omega_0 = (0,0,1)^{\mathrm{T}}$, hence $\mu_0 = 1$ in Eq. (25), then we have

$$F_x(\tau_z) = F_y(\tau_z) \equiv 0 \tag{44}$$

for any z, any τ, and phase function. Figure 1b illustrates the flux lines—the mean photon flow—for this highly symmetric situation. In the case of slant illumination ($\mu_0 < 1$), we have

$$F_x(H) = \int_{\Xi} \Omega_x I(H,\Omega)\, \mathrm{d}\Omega = \sum_{i=1}^{4} \int_{i\text{'th quadrant}} \Omega_x I(H,\Omega)\, \mathrm{d}\Omega \ . \tag{45}$$

Referring to the schematic of the principal plane in Fig. 2, we see that contributions from quadrants 2 and 3 ($\Omega_z < 0$) come from the BCs in Eqs. (25) and (28): quadrant 2 ($\Omega_x \geq 0$) gives zero as soon as the sun is off-zenith ($\Omega_{x_0} > 0$, $\Omega_{y_0} = 0$ because $\varphi_0 = 0$, and $\Omega_{z_0} = \mu_0 < 1$), and quadrant 3 ($\Omega_x < 0$) yields $-(1-\mu_0^2)^{1/2} \times F_0$. Contributions from quadrants 1 and 4 ($\Omega_z \geq 0$) are determined by the RTE's solution; in general, they are of unequal magnitude, but if the scattering is rigorously isotropic, then they are equal in magnitude and opposite in sign, so they cancel in Eq. (31). In summary, we have $F_x(H) < 0$. Conditional that $(1-g)\tau \gg 1$ then, for any Ω_0 in the principal ($y = constant$) plane represented in Fig. 2, there exists[37] a diffusion domain deep enough inside M, where

$$\begin{cases} F_x(\tau_z) \approx 0 \ , & constant/(1-g) \lesssim \tau_z \leq \tau \\ F_y(\tau_z) = 0 \ , & 0 \leq \tau_z \leq \tau \end{cases} . \tag{46}$$

The value assigned to the numerical constant will depend on the criterion for the onset of diffusive transport; van de Hulst[27] argues for two.

Although there are three spatial dimensions in HPP theory, it is often referred to as 1D theory because of the mathematical structure of Eq. (42). Furthermore, there is a large class of two-stream approximations to HPP theory,[46] an idea that actually antedates the RTE itself.[47] Basically, one captures the effects of absorption ($\varpi_0 \leq 1$), forward scattering ($g \geq 0$), and/or slant illumination ($\mu_0 \leq 1$) in the various coefficients that appear in a tractable system of two coupled ordinary differential equations (ODEs). This leads to closed-form results for T, R, and A as functions of $(\mu_0, \varpi_0, g, \tau)$.

IV.B. Steady-State Diffusion in a Homogeneous Slab

An approximation akin to the two-stream model is obtained by applying photon diffusion theory to a homogeneous slab. We end up solving an ODE in $J(z)$, $[-(\mathrm{d}/\mathrm{d}z)^2 + 3(1-\varpi_0)(1-\varpi_0 g)\sigma^2]J = 0$ with BCs in Eq. (31), where μ_0 does not appear explicitly (i.e., separated from F_0). In the conservative case ($\varpi_0 = 1$), we solve a 1D Laplace equation, $-(\mathrm{d}/\mathrm{d}z)^2 J = 0$. So we have $J(z) = J_0 + J'z$, where we obtain $J_0 = \mu_0 F_0 T_{\mathrm{HPP}}$ from Eq. (34b); J' is obtained from the lower BC in (31): $J_0 - \chi \ell_{\mathrm{t}} J' = 0$. We find

$$J(z) = \mu_0 F_0 \times T_{\mathrm{HPP}} \times (1 + z/\chi\ell_{\mathrm{t}}) \ . \tag{47}$$

As remarked earlier, the constant magnitude of the flux vector, $|F_z| = (\ell_{\mathrm{t}}/3)J'$ from Fick's law in Eqs. (13) and (14), is $T_{\mathrm{HPP}}/3\chi$. The key quantity here is the transmittance of the slab:

$$T_{\mathrm{HPP}}(\mu_0, 1, g, \tau) = 1 \Big/ \left[1 + \frac{H}{2\chi\ell_{\mathrm{t}}}\right] , \tag{48a}$$

where the nondimensional term contains the dependencies on optical parameters,

$$\frac{H}{2\chi\ell_{\mathrm{t}}} = \frac{(1-g)\tau}{2\chi} = \frac{3}{4}(1-g)\tau \tag{48b}$$

if we opt for $\chi = 2/3$ in Eq. (32).

Unlike the aforementioned result, the popular versions of two-stream theory account approximately for direct solar beam effects as μ_0 varies over the Earth's surface. The simplest model is[20]

$$T_{\mathrm{HPP}}(\mu_0,1,g,\tau) = 1\Big/\left[1+\frac{(1-g)\tau}{2\mu_0}\right] , \qquad (49)$$

which coincides with Eqs. (48a) and (48b) when $\mu_0 = \chi = 2/3$ ($\theta_0 = 53.5$ deg). Meador and Weaver[46] describe several increasingly sophisticated formulations of the two-stream model. To incorporate the nontrivial effects of μ_0 in the framework of diffusion theory, one would use J only to model the diffuse component and therefore solve the aforementioned ODE with homogeneous BCs and a source term for direct transmission. The outcome is somewhat more complex than Eqs. (47) and (48) in that exponentials are present, even for $\varpi_0 = 1$.

IV.C. One-Half-Order Solution for Large-Scale Properties: Linear Mixing of Cloudy and Clear Skies

An important meteorological application of HPP theory is to compute (approximately but efficiently) the contribution of solar radiation to the energy budget at all levels in the atmospheric column. It is unrealistic, however, to expect the atmosphere to be horizontally homogeneous at the relatively large scales of interest in numerical climate modeling (grid points are several hundred kilometres wide). The simplest possible characterization of subgrid scale variability is to somehow define a cloud fraction N. We then mix results for cloudy and clear skies as follows:

$$F_{\mathrm{eff}}(z) = \mu_0 F_0 \times \begin{cases} [NT_{\mathrm{cloud}} + (1-N)T_{\mathrm{clear}} - 0 , & z = 0 \\ 1 - [NR_{\mathrm{cloud}} + (1-N)R_{\mathrm{clear}}] , & z = H \end{cases} \qquad (50)$$

for the net fluxes at the boundaries. Typically, two-stream approximations as in Eqs. (48) or (49) are used to obtain the R's and T's, sometimes an accurate solution of the 1D RTE in Eq. (42).

Since there is no account of horizontal fluxes, nor of the generally continuous distribution of optical depth values, we consider this computational device as part of HPP theory, only a half-step toward accommodating horizontal variability. We will call the result in Eq. (50) weighted plane-parallel (WPP) theory.

V. FIRST-ORDER SOLUTION: THE INDEPENDENT PIXEL APPROXIMATION

V.A. Enforced Local Translational Symmetry (Adapting to Horizontal Variability)

Remaining with the albedo problem, Eq. (25), in plane-parallel geometry, Eq. (26), we maintain the identification of both x and y derivatives with zero, Eq. (41), from Sec. IV.A. However, instead of neglecting horizontal variability altogether, as in Eq. (40), we rather make the following identification:

$$\sigma(\boldsymbol{x}) \equiv \sigma(x,y;z) , \qquad (51)$$

where the semicolon now separates the independent variable z from the parameters x and y. Indeed, only z is used in solving the RTE in HPP geometry. More precisely, we continue to use HPP theory but with an optical thickness that is (x,y)-dependent:

$$\tau(x,y) = \int_0^H \sigma(x,y;z)\,\mathrm{d}z . \qquad (52)$$

Cahalan et al.[48] call this the independent pixel approximation (IPA). Figure 1c illustrates diffusive transport under the IPA assumption. In comparison with HPP theory in Fig. 1b, flux lines are still parallel to one another and perfectly aligned along the vertical axis; however, they are no longer equidistant. We are now dealing with a local symmetry.

V.B. Pixel-Scale Values and Coarse-Graining

At some fine (pixel) scale, we use HPP theory to compute

$$F_{\mathrm{IPA}}(x,y) = F_{\mathrm{HPP}}[\cdot,\tau(x,y)] \qquad (53)$$

for any radiative quantity of interest: a reflectance ($F = R$), a transmittance ($F = T$), or an absorptance ($F = A$), possibly a radiance ($F = I$), etc.; these will in general depend on the usual geometric and optical parameters (μ_0, ϖ_0, g). For instance, we can use results from 1D diffusive (or two-stream) transport theory in slab geometry, namely, Eqs. (48a) and (48b) or Eq. (49) for $F = T$ and $\varpi_0 = 1$.

The general question of IPA validity at small scales is discussed in Sec. VIII. In practice, the IPA is used to compute larger-scale quantities by coarse-graining the radiative response in Eq. (53):

$$\bar{F}_{\mathrm{IPA}}(r;x,y) = \frac{1}{r^2}\int_x^{x+r}\int_y^{y+r} F_{\mathrm{HPP}}[\cdot,\tau(x',y')]\,\mathrm{d}y'\,\mathrm{d}x' . \qquad (54)$$

This whole strategy is based on the hope that for a large enough scale r, $\bar{T}_{\mathrm{IPA}}(r;\cdot)$, $\bar{R}_{\mathrm{IPA}}(r;\cdot)$ and $\bar{A}_{\mathrm{IPA}}(r;\cdot)$ become reasonable approximations to the exact coarse-grained quantities in Eqs. (37a), (37b), and (37c) in the macroscopic radiative budget spelled out in Eq. (38). At this scale, the contribution of horizontal fluxes, $\bar{\Delta}(r;\cdot)$ in Eq. (39), should be negligibly small because $\bar{\Delta}_{\mathrm{IPA}}(\cdot) = 1 - \bar{T}_{\mathrm{IPA}}(\cdot) - \bar{R}_{\mathrm{IPA}}(\cdot) - \bar{A}_{\mathrm{IPA}}(\cdot) \equiv 0$.

V.C. Random τ Events and Ensemble-Averaging

The power of the IPA method is twofold:

1. It is computationally efficient compared to any exact method of solving the full 3D RTE, even in the diffusion approximation, and even if this is repeated many times at the pixel scale.

2. The IPA averages in Eq. (54) can often be obtained for r large enough in closed form,[49] as long as one more hypothesis is clearly stated.

The new hypothesis is similar to ergodicity in the statistical literature: We replace the spatial average in Eq. (54) by an ensemble average. In practice, this means that instead of summing à la Riemann over all possible pixels, each with the same weight, we sum à la Lebesgue over all possible τ values (events), weighting each one by its relative frequency in the ensemble of all possible realizations. In other words, we integrate Eq. (53) with respect to the probability measure

$$\begin{aligned} \mathrm{d}P(\tau) &= P(\mathrm{d}\tau) \\ &= \mathrm{Prob}\{\tau \le \textit{optical thickness} < \tau + \mathrm{d}\tau\} \ . \end{aligned} \tag{55}$$

We will use $P(\tau)$ to denote Prob$\{0 \le$ *optical thickness* $\le \tau\}$, the cumulative probability of τ. The probability density function (pdf) of τ is $\mathrm{d}P/\mathrm{d}\tau$ when it exists.

Dropping the (presumably weak) spatial and scale dependencies in Eq. (54), we have

$$\bar{F}_{\mathrm{IPA}} \approx \langle F_{\mathrm{HPP}}(\tau)\rangle = \int_0^\infty F_{\mathrm{HPP}}(\tau)\,\mathrm{d}P(\tau) \ . \tag{56}$$

The WPP scheme for large-scale fluxes in Eq. (50) offers a simple illustration of the IPA concept using a probability measure for τ. Specifically, there are only two types of pixel (cloudy and clear), drawn at random from a Bernoulli law: Prob{cloudy} = N, and Prob{clear} = $1 - N$; Eq. (50) then follows directly from Eqs. (55) and (56).

Equation (56) immediately explains a well-known effect of horizontal variability: systematic albedo reduction. Notice how we have more flux lines in Fig. 1c (IPA schematic) than in Fig. 1b (HPP schematic). This is not arbitrary and translates graphically the fact that the overall flux (hence transmittance) through the system is increased in the improved theory (so albedo is reduced). This is a direct consequence of Jensen's inequality,[50] namely,

$$\langle F(\tau)\rangle \ge F(\langle\tau\rangle) \tag{57}$$

as soon as $F(\tau)$ is convex, i.e., $F''(\tau) \ge 0$ over the support of $P(\tau)$, i.e., the $\mathcal{R}$ domain, where $0 < P < 1$. The = is obtained in Eq. (57) in only two cases:

$$F(\tau) = a\tau + b \ ;$$

or

$$P(\tau) = \Theta(\tau - \langle\tau\rangle) \ ,$$

where $\Theta(\cdot)$ is the Heaviside step function.

For illustration, one can average the direct transmission through the sine-wave cloud model in Eq. (27): use Eq. (56) with $F(\tau) = T_{\mathrm{dir}}(\tau) = \exp(-\tau)$ and $P(\tau)$, which is $\cos^{-1}[(\langle\tau\rangle - \tau)/\delta\tau_{\max}]/\pi$ on the interval $[\langle\tau\rangle - \delta\tau_{\max}, \langle\tau\rangle + \delta\tau_{\max}]$, 0 before and 1 after. Equivalently, use Eq. (54) with $r = L$ and a trivial change in variables to show that

$$\langle T_{\mathrm{dir}}(\tau)\rangle = \int_0^\pi \exp[-(\langle\tau\rangle - \delta\tau_{\max}\cos\varphi)]\,\mathrm{d}\varphi/\pi \ .$$

This yields

$$\langle T_{\mathrm{dir}}(\tau)\rangle = \exp(-\langle\tau\rangle) I_0(\delta\tau_{\max}) \ , \tag{58}$$

where $I_0(\cdot)$ is the order-0 modified Bessel function; so $\langle T_{\mathrm{dir}}(\tau)\rangle / T_{\mathrm{dir}}(\langle\tau\rangle) = I_0(\delta\tau_{\max})$ is unity at the origin and increases monotonically on $\mathcal{R}^+$, as predicted in (57).

Since $(\partial/\partial\tau)^2 T > 0$ for $\tau \ge 0$ in Fig. 3a, we can anticipate $\langle T(\tau)\rangle \ge T(\langle\tau\rangle)$ for any μ_0, ϖ_0, and g. Similarly, the IPA average of reflectance, e.g., $R_{\mathrm{HPP}}(\tau) = 1 - T(\mu_0, 1, g, \tau) = (1-g)\tau/[2\mu_0 + (1-g)\tau]$ from the two-stream result in Eq. (49), will lead to a value smaller than $R_{\mathrm{HPP}}(\langle\tau\rangle) \equiv R(\mu_0, 1, g, \langle\tau\rangle)$ because $(\partial/\partial\tau)^2 R < 0$. Cahalan et al.[51] call

$$\begin{aligned} \delta R_{\mathrm{IPA}} &= \bar{R}_{\mathrm{IPA}} - R_{\mathrm{HPP}}(\langle\tau\rangle) \\ &\approx \langle R_{\mathrm{HPP}}(\tau)\rangle - R_{\mathrm{HPP}}(\langle\tau\rangle) \le 0 \end{aligned} \tag{59}$$

the plane-parallel bias; it is necessarily negative because the reverse inequality from Eq. (57) applies here.

Figure 3b shows $|\delta R_{\mathrm{IPA}}|$ for a specific example, the smoothly varying sine-wave cloud model in Eq. (27) and Fig. 1. Any $T_{\mathrm{HPP}}(\tau) = 1 - R_{\mathrm{HPP}}(\tau)$ in the form $1/[1 + \textit{constant} \times \tau]$ as, e.g., in Eqs. (48) or (49). A little algebra then yields $\langle T_{\mathrm{HPP}}(\tau)\rangle / T_{\mathrm{HPP}}(\langle\tau\rangle) = [1 - a^2]^{-1/2} \ge 1$, where $a = R_{\mathrm{HPP}}(\langle\tau\rangle) \times \delta\tau_{\max}/\langle\tau\rangle$; the range of this parameter is $0 \le a \le R_{\mathrm{HPP}}(\langle\tau\rangle) < 1$. Notice how the resulting albedo bias is maximum when the variance of τ is the largest possible and when $\langle\tau\rangle$ is at a point (dependent on the adopted variability model) that maximizes the effect of $R_{\mathrm{HPP}}(\tau)$'s nonlinearity with respect to τ. If the pdf is heavily weighted by very large τ values, where $R_{\mathrm{HPP}}(\tau)$ is almost saturated at unity, the bias will necessarily decrease. It is interesting to note that with the typical optical parameters used in cloud studies ($g = 0.85$, $\chi = 2/3$) and relatively strong variability ($0.7 \lesssim \delta\tau_{\max}/\langle\tau\rangle \lesssim 1$), the largest albedo biases (>0.05) are reached precisely at typical values of $\langle\tau\rangle$, from $\approx$10 to $\approx$50.

V.D. Application to Earth's Climate System

It is now widely acknowledged by the meteorological community that variable cloud systems transmit more visible sunlight than their homogeneous counterparts for a given amount of total liquid water, at least for nongrazing incidence. As described in Sec. V.C, the IPA

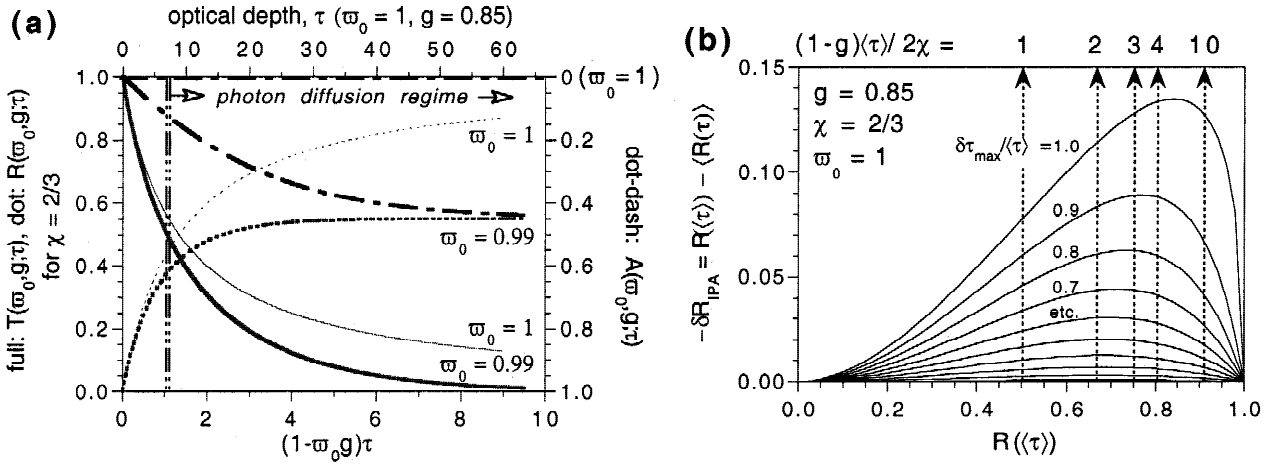

Fig. 3. IPA tools and case study. (a) Taking $\chi = 2/3$ from Eq. (32), we plot on the left axis $T_{\mathrm{HPP}}(\varpi_0, g; \tau)$ and $R_{\mathrm{HPP}}(\varpi_0, g; \tau)$ versus $(1 - \varpi_0 g)\tau$ for $g = 0.85$ with $\varpi_0 = 1$ (e.g., clouds in the visible spectrum) and $\varpi_0 = 0.99$ (e.g., clouds in near IR). In the former (conservative scattering) case, we have $T_{\mathrm{HPP}}(1, g; \tau) + R_{\mathrm{HPP}}(1, g; \tau) \equiv 1$, $A_{\mathrm{HPP}}(1, g; \tau) \equiv 0$; in the absorbing case, we also plot $A_{\mathrm{HPP}}(\varpi_0, g; \tau)$ on the right axis. We have highlighted the regime where diffusion theory (and related two-stream approximations) work best: $(1 - \varpi_0 g)\tau \gtrsim 1$, meaning $\tau \gtrsim 6$ to 7 for dense boundary-layer clouds ($g \approx 0.85$, $\varpi_0 \approx 1$). Note that $T_{\mathrm{HPP}}(\varpi_0, g; \tau)$ is convex with respect to τ, whereas $R_{\mathrm{HPP}}(\varpi_0, g; \tau)$ and $A_{\mathrm{HPP}}(\varpi_0, g; \tau)$ are concave; these analytical properties are characteristic of diffusive transport and explain the systematic effects of variability discussed in the main text. (b) We plot the plane-parallel bias $|\delta R_{\mathrm{IPA}}|$ from Eq. (59) for the sine-wave extinction field in Fig. 1 and Eq. (27) as a function of $R_{\mathrm{HPP}}(\cdot; \langle\tau\rangle)$ for conservative scattering ($\varpi_0 = 1$); also indicated (upper axis) are some representative values of the domain-average optical depth $\langle\tau\rangle$ rescaled by $2\chi/(1 - g) \approx 8.9$ for the typical values used in Fig. 3a. The bias increases with the variability parameter $\delta\tau_{\max}/\langle\tau\rangle \leq 1$ and with $\langle\tau\rangle$ although only up to a point determined by $\delta\tau_{\max}/\langle\tau\rangle$.

approach to radiative transfer at large scales elegantly explains this in conjunction with two-stream—hence diffusion-type—radiation transport theory.

The resulting albedo bias in the 5 to 10% range (with respect to $\mu_0 F_0$) seems small until one realizes how much that modulates the sole energy source of the climate system, which is in a close radiative equilibrium. Solar flux at the Earth's orbit is $F_0 \approx 1370$ W/m^2, and spread over the whole globe (including night side), this input is still $\langle\mu_0\rangle F_0/2 \approx 342$ W/m^2 on average (a typical value at midlatitudes). Approximately 30% of this energy budget is reflected back to space (largely thanks to clouds), but a 5 to 10% fluctuation is still 17 to 34 W/m^2. This is the number to be contrasted with the mere 4 to 5 W/m^2 increase in surface heating (by enhanced greenhouse effect) that would result from an anthropogenic doubling of CO_2 in the atmosphere. The corresponding changes in surface temperature, sea level, cloudiness, etc., depend of course on feedback mechanisms, poorly understood for the most part. Some of these feedbacks are mediated by clouds, so cloud-radiative processes need to be adequately represented in global climate models (GCMs), including the effects of 3D structure if possible. New solar cloud-radiation modules in GCMs that incorporate the IPA (effects beyond the linear mixing described in Sec. IV.C) are in order and some are currently being tested.[49,52]

VI. SECOND-ORDER SOLUTION: THREE-DIMENSIONAL DIFFUSION THEORY

VI.A. Symmetry Broken (Welcoming Horizontal Variability)

In the previous two sections, we have discussed media where there is no cause for net horizontal fluxes to arise (HPP, Sec. IV) and a computational device (IPA, Sec. V) where we neglect horizontal fluxes but allow for the variability that will surely excite them. We now turn to radiation transport models that fully account for horizontal fluxes. Figure 1d illustrates schematically this desire with the simple sine-wave medium from Fig. 1 and Eq. (27), already used in Secs. IV and V. In the remainder of this section, 3D diffusion theory is used to describe the mechanics of extinction-radiance interaction; we will follow Cannon[53] and refer to the dominant process as radiative channeling.

Figure 1d shows the tendency of photons to flow around the dense central area and into the more tenuous regions on either side, an example of radiative channeling (Sec. VI.B and Fig. 4 in Sec. VI.B). The fact that the flux lines are more evenly spread out at the lower boundary than the upper one, where the photons originate, is not arbitrary; this is caused by the more extensive radiative smoothing in transmittance than in reflectance, as explained in Sec. VIII.

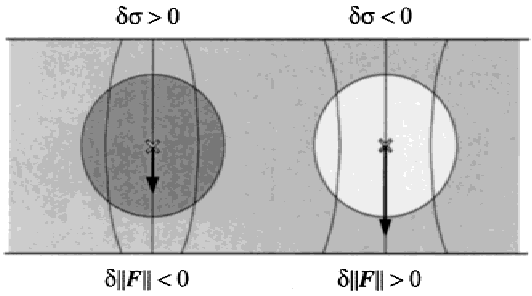

Fig. 4. Radiative channeling. An originally homogeneous plane-parallel medium is restructured internally by removing scattering material from the circular region highlighted on the right side and adding it to the region on the left side. Flux lines are naturally deflected around the dense region and into the tenuous one. Flux-line geometry used here assumes diffuse or, if collimated, normal illumination (see discussion of Fig. 2).

VI.B. Local Analysis: Radiative Channeling as the Symmetry-Breaking Mechanism

In this section, we take $\sigma_a(\boldsymbol{x}) \equiv 0$ in Eqs. (3) and (4), hence $\sigma(\boldsymbol{x}) = \sigma_s(\boldsymbol{x})$ and $\varpi_0 = 1$ in Eq. (5). Substitution of Fick's law [Eq. (13)] and the expression for radiative diffusivity in Eqs. (14) and (15) into Eq. (12) leads under these conditions to[4]

$$\nabla^2 J = [\nabla \ln \sigma]\cdot[\nabla J] \ , \tag{60}$$

so J responds only to the relative fluctuations of $\sigma(\boldsymbol{x})$: $\nabla \ln \sigma = (\nabla\sigma)/\sigma$. Even with the BC effects discussed later, this remains largely true. Equation (60) is easier to interpret in the form

$$-\nabla^2 J = 3(1-g)\boldsymbol{F}(\boldsymbol{x})\cdot\nabla\sigma \ , \tag{61}$$

bearing in mind the other $\boldsymbol{F} - \sigma - J$ coupling in Fick's law

$$\boldsymbol{F}(\boldsymbol{x}) = -[3(1-g)\sigma(\boldsymbol{x})]^{-1}\nabla J \ . \tag{62}$$

Let $J_{\mathrm{HPP}}(\boldsymbol{x}) \equiv J_{\mathrm{HPP}}(z)$ be the solution of Laplace's equation

$$-\nabla^2 J_{\mathrm{HPP}} = 0 \tag{63}$$

with the BCs in Eq. (31). In this homogeneous situation, $\boldsymbol{F}_{\mathrm{HPP}}(\boldsymbol{x})$ is a uniform vector field; furthermore, the only nonvanishing component is $(F_z)_{\mathrm{HPP}} \equiv -\mu_0 F_0 T_{\mathrm{HPP}}/3\chi$. The constant T_{HPP} is transmittance, as obtained from g and $\bar{\tau} = \bar{\sigma}H$ in Eqs. (48a) and (48b). We use here volume-averaged extinction:

$$\bar{\sigma} = \int_M \sigma(\boldsymbol{x})\,\mathrm{d}\boldsymbol{x} \Big/ \int_M \mathrm{d}\boldsymbol{x} = \frac{1}{HL^2}\int_M \sigma(\boldsymbol{x})\,\mathrm{d}\boldsymbol{x} \tag{64}$$

because

$$\mathrm{M} = [0,L)^2 \otimes (0,H) \tag{65}$$

is the (periodically replicated) computational domain of interest in the following. Let

$$\sigma(\boldsymbol{x}) = \bar{\sigma} + \sigma'(\boldsymbol{x}) \tag{66}$$

define the extinction fluctuation $\sigma'(\boldsymbol{x})$; by this definition, the average of $\sigma'(\boldsymbol{x})$ over M vanishes. Also let

$$\begin{cases} J(\boldsymbol{x}) = J_{\mathrm{HPP}}(z) + J'(\boldsymbol{x}) \\ \boldsymbol{F}(\boldsymbol{x}) = \boldsymbol{F}_{\mathrm{HPP}}(z) + \boldsymbol{F}'(\boldsymbol{x}) \end{cases} , \tag{67}$$

where $J(\boldsymbol{x})$ is the solution of Eq. (60), with BCs in Eq. (31), and $\boldsymbol{F}(\boldsymbol{x})$ is derived from Fick's law in Eq. (62). These quantities are decomposed in the same way as $\sigma(\boldsymbol{x})$ in Eq. (66), but without any prior knowledge about their volume integrals (they are in fact estimated later).

From Eqs. (61) and (67), we see that the 3D component of the solution, $J'(\boldsymbol{x})$, obeys exactly

$$-\nabla^2 J' = 3(1-g)\boldsymbol{F}(\boldsymbol{x})\cdot\nabla\sigma \tag{68}$$

with BCs in z as in Eq. (31) but homogeneous, i.e., vanishing right sides (a fact we will exploit later). [The inhomogeneous part of the BC for $J(\boldsymbol{x})$ at $z = H$ is readily accounted for in the zeroth-order HPP solution.] Furthermore, in contrast with Eq. (63) for the unperturbed field, $J'(\boldsymbol{x})$ has an internal source-and-sink-like term on the right side of Eq. (68) [see Eq. (11) with $\partial/\partial t \equiv 0$].

Retaining only first-order terms in $\nabla\sigma \equiv \nabla\sigma'$, J', $\boldsymbol{F}'$ from Eq. (68), we find

$$\begin{aligned} -\nabla^2 J' &\approx 3(1-g)\boldsymbol{F}_{\mathrm{HPP}}\cdot\nabla\sigma \\ &= \left[0\times\frac{\partial}{\partial x} + 0\times\frac{\partial}{\partial y} - 3(1-g)\mu_0 F_0 T_{\mathrm{HPP}}\times\frac{\partial}{\partial z}\right] \\ &\quad \times \sigma(\boldsymbol{x}) \end{aligned} \tag{69}$$

and defer to Sec. VI.C a discussion of the magnitude of the neglected terms. The schematic in Fig. 4 illustrates the fate of flux-line geometry, as dictated by Eq. (69), when scattering material is added and/or removed to an HPP substrate. Recalling that extinction is proportional to local particle density, we see that

1. where the extinction or density gradient is in the opposite direction from the unperturbed (and overall) flux, the right side of Eq. (69) is negative. The perturbed flux lines will therefore appear in a converging pattern. To see this in a simple way, note that $\nabla\cdot\boldsymbol{F}' \propto -\nabla^2 J'$ will also be <0, i.e., the same sign as the characteristic sink term in Eq. (11). There are examples in the lower left and upper right parts of Fig. 4.

2. where the gradients are in the same direction as the average flux [the right side of Eq. (69) is >0], the perturbed flux lines will then diverge from each other because $\nabla\cdot\boldsymbol{F}' > 0$ then looks like the internal source term in Eq. (11). (See upper left and lower right portions of Fig. 4.)

3. elsewhere, there is little variation in $\sigma(\boldsymbol{x})$ along the mean flux line [so the right side of Eq. (69) is ≈ 0]. In this case, flux lines are in a locally parallel/equidistant configuration; see, for instance, the portion of Fig. 4 midway between the two boundaries.

Overall, we see that the response of the photon flow to a positive fluctuation in extinction (density) is to deflect itself around the correspondingly opaque region. In the same manner, photons will tend to flow toward and into the tenuous region related to a negative fluctuation in $\sigma(\boldsymbol{x})$. Although in a different setting (spectral line transfer), Cannon[53] described a similar phenomenon observed in his early 2D numerics: "[photons flow] into the less opaque regions by increased scattering in the regions of greater opacity;" he called this radiative channeling. In particular, channeling is responsible in Fig. 1d (3D diffusion transport) for breaking the translational symmetry in the vertical direction in Fig. 1c (IPA transport).

IV.C. Global Analysis: The Effect of Variability on Bulk Transport Properties

We carry on the aforementioned 3D perturbation analysis by incorporating BCs. We wish to determine a global quantity such as $T(r,\cdot)$ in Eq. (37b), where the averaging-scale r is, in principle, large enough that we can neglect the residual dependence on the horizontal coordinates.[c] In practice, we just take $r = L$, the size of the finite horizontal computational domain in Eq. (69), where we apply periodic BCs in the horizontal plane. The transport problem is specified entirely in the framework of the plane-parallel geometry defined in Eqs. (25) and (28).

Now, define the global responses to an arbitrary perturbation in the extinction field:

$$\delta R = \bar{R}(L,\cdot) - R_{\mathrm{HPP}} \tag{70a}$$

or

$$\delta T = \bar{T}(L,\cdot) - T_{\mathrm{HPP}} = -\delta R \ , \tag{70b}$$

because we are in the framework of conservative scattering. Of the 3D perturbation, we require only that

1. $\sigma(\boldsymbol{x}) = \bar{\sigma} + \sigma'(\boldsymbol{x}) \geq 0$
2. the integral of $\sigma'(\boldsymbol{x})$ over M vanishes, as follows from Eqs. (64) and (66).

This latter requirement is akin to conservation of total mass, equivalently, of the total number of scattering particles, because extinction is proportional to the local density of the scattering material. Any scattering mass redistribution compatible with the former constraint is acceptable; in particular, we do not need $\sigma'(\boldsymbol{x})$ to be small in any sense.

Substitution of the mean+deviation decomposition in Eqs. (56) and (57) into Fick's law in Eq. (62), rewritten for more convenience as $[3(1-g)\sigma(\boldsymbol{x})]\boldsymbol{F}(\boldsymbol{x}) = -\nabla J$, yields

$$3(1-g)\bar{\sigma}\boldsymbol{F}_{\mathrm{HPP}} = -\nabla J_{\mathrm{HPP}} \tag{71}$$

at zeroth order, and

$$3(1-g)[\sigma' F_{z\mathrm{HPP}} + \bar{\sigma}F_z' + \sigma' F_z'] = -\left(\frac{\partial}{\partial z}\right) J' \tag{72}$$

for all the perturbation terms along the (vertical) z axis.

We now integrate Eq. (72) term-by-term over M and divide by the total incoming flux, $\mu_0 F_0 L^2$:

1. *First term in Eq. (72)*: It vanishes identically because of the aforementioned mass-conservation constraint.

2. *Second term in Eq. (72)*: We exploit the fact that the total flux crossing a horizontal cut through M is invariant in z. This follows directly from radiant energy conservation, $\nabla\cdot\boldsymbol{F} = 0$, and applies to the perturbation term as well: $\nabla\cdot\boldsymbol{F}' = 0$ (because $\nabla\cdot\boldsymbol{F}_{\mathrm{HPP}} = 0$). So we only need to estimate the horizontal integral once: at $z = 0$, we have $F_z(x,y,0) = -\mu_0 F_0 T(x,y)/3\chi$ from Sec. IV.B. The perturbation of its spatial integral is therefore $-\mu_0 F_0 L^2 \delta T/3\chi$, using Eqs. (37b) and (70b). After vertical integration and normalization, the second term in Eq. (72) thus becomes $-3(1-g)\bar{\sigma}H\delta T/3\chi = -(1-g)\bar{\tau}\delta T/\chi$.

3. *Third term in Eq. (72)*: It simply yields $3(1-g)H \times \overline{\sigma' F_z'}/(\mu_0 F_0)$, where the (one-point) covariance of the fluctuations in extinction and in vertical flux is measured by

$$\overline{\sigma' F_z'} = \frac{1}{HL^2}\int_M \sigma'(x) F_z'(\boldsymbol{x})\,\mathrm{d}\boldsymbol{x} \ . \tag{73}$$

Multiplying top and bottom by $\bar{\sigma}$, the third term becomes $3(1-g)\bar{\tau} \times \overline{\sigma' F_z'}/(\bar{\sigma}\mu_0 F_0)$.

4. *Right side of Eq. (72)*: Being the volume-integral of a gradient in z, this becomes the difference between the horizontal integrals of $J'(\boldsymbol{x})$ taken at $z = 0$ and $z = H$. Using Eqs. (34a), (34b), (37a), and (37b), this becomes the difference between δR obtained at $z = 0$ and $\delta T = -\delta R$ obtained at $z = H$. The right side of Eq. (72) thus becomes $-2\delta R = 2\delta T$. In summary, Eq. (72) has become

$$-(1-g)\bar{\tau}\delta T/\chi + 3(1-g)\bar{\tau}\,\frac{\overline{\sigma' F_z'}}{\bar{\sigma}\mu_0 F_0} = 2\delta T \ . \tag{74}$$

Grouping similar terms, we can solve for δT. Using Eqs. (48a) and (48b), we recognize the multiplier of δT as $1/(3\chi R_{\mathrm{HPP}}) = 1/[3\chi(1-T_{\mathrm{HPP}})]$. Thus we can rewrite Eq. (74) as

$$\frac{\delta T}{1-T_{\mathrm{HPP}}} = \frac{-\delta R}{R_{\mathrm{HPP}}} = 3\chi\,\frac{\overline{\sigma' F_z'}}{\bar{\sigma}\mu_0 F_0} \ . \tag{75}$$

[c] We are in an effectively ergodic regime.

The preceding formula for δT is exact in the framework of diffusion theory and it is second order in the fluctuations. In other words, the quantity δT vanishes in the limit of a linear perturbation analysis, as used locally in Eq. (69). We also see that—as predicted from Eq. (60)—only the relative fluctuations, $\sigma'/\bar{\sigma}$, are important in diffusion theory. Finally, the magnitude of δT will depend on the specifics of the perturbation, but we can predict its sign on general grounds: $\delta T > 0$.

Proof that $\delta T > 0$: We only need to consider the numerators in Eq. (75). Flux lines define the flux-vector field completely up to a multiplicative constant: At a given point, its direction is given by the tangent of the line through that point and its magnitude by the local density of lines (number of lines piercing a unit surface at right angles to the tangent) (see Figs. 1b through 1d). Thus, if $\delta\sigma = \sigma' > 0$ (left side of Fig. 4), then $\delta\|\boldsymbol{F}\| = -F_z' < 0$, because perturbed lines are the furthest apart here; conversely, if $\delta\sigma = \sigma' < 0$ (right side of Fig. 4), then $\delta\|\boldsymbol{F}\| = -F_z' > 0$, because perturbed lines are closer here. In summary, we can safely assert that the numerator on the right side of Eq. (75) is positive; hence, $\delta T > 0$. Davis[9] provides another argument, using Stephens's parameterized representation[54] of his numerical results.[55]

VI.D. Relation of Eq. (75) to the Independent Pixel Approximation and Sun-Angle Complications

In the framework of the IPA, we can define in analogy with Eq. (59)

$$\delta T_{\mathrm{IPA}} = \overline{T}_{\mathrm{IPA}} - T_{\mathrm{HPP}}(\bar{\tau}) = \overline{T_{\mathrm{HPP}}(\tau)} - T_{\mathrm{HPP}}(\bar{\tau}) \ , \quad (76)$$

and we found that

$$\delta T_{\mathrm{IPA}} = -\delta R_{\mathrm{IPA}} \geq 0 \quad (77)$$

as a consequence of Jensen's inequality in Ref. 55. How does this bias compare to the general definition of δT in Eq. (70b) and its 3D diffusion-based estimate in Eq. (75)?

Imagine a medium where $\tau(x, y) \equiv \bar{\tau}$ in Eq. (52); yet, every column has a different structure in z. Such a medium has $\delta T_{\mathrm{IPA}} = 0$ in Eq. (77), yet horizontal fluxes will occur, so $\delta T > 0$ in Eqs. (70b) and (75). Based on this example, we conjecture that in diffusion theory for pure scattering ($\varpi_0 = 1$), we have

$$\delta T \geq \delta T_{\mathrm{IPA}} \geq 0 \quad (78)$$

and, from there,

$$T \geq T_{\mathrm{IPA}} \geq T_{\mathrm{HPP}}(\bar{\tau}) \quad (79)$$

for any $\sigma(\boldsymbol{x})$ in plane-parallel geometry that conserves mass (same $\bar{\tau}$). Returning to Fig. 1, this explains why, realistically, there are more flux lines in Fig. 1c than in Fig. 1b and more in Fig. 1d than in Fig. 1c.

The conditions under which the ordering in Eq. (79) carries over to RTE solutions are an open question. In meteorological applications, sun angle $\theta_0 = \cos^{-1}\mu_0$ is an important parameter and, given the huge range of extinction found in the atmosphere, deviations from diffusion theory need to be addressed. For all practical purposes, illumination is regarded as isotropic in diffusion theory as used here with BCs in Eq. (31); along with F_0, μ_0 controls the strength of the illumination but not its directivity.[d] It seems natural to require that the illumination be at least as symmetric as the $\sigma(\boldsymbol{x})$ field in order to obtain the ordering in Eq. (79). Going back to Fig. 2, it is easy to see that another (illumination-symmetric) situation that is easier to comprehend is when $\mu_0 = 1$, but, strictly speaking, it is only applicable to one (subtropical) location on Earth at a time. The first inequality in Eq. (79) has indeed been observed to occur in the reverse order in numerical simulations, only when $\mu_0 < 1$ however. For instance, the Monte Carlo estimates of the IPA bias $R_{\mathrm{IPA}} - R = T - T_{\mathrm{IPA}}$ by Cahalan et al.[51] are of either sign, dependent on μ_0 and cloud variability parameters.

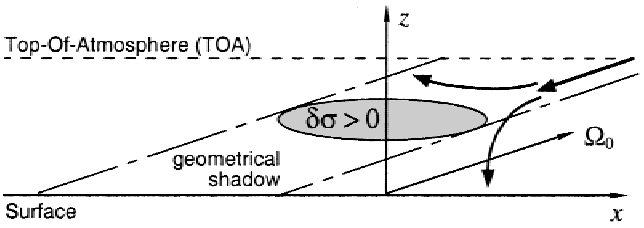

Fig. 5. Radiative channeling when $\mu_0 < 1$ described schematically by typical radiative flux lines. Channeling of photon flow contributes here to both reflectance and transmittance, whereas in Fig. 4 only the latter benefits on average, as a second-order correction to the HPP case (see Sec. VI.C). Whatever the configuration, photons interact collectively with the fluctuations of the extinction field like a fluid in a porous medium,[56] always seeking channels (paths of least resistance).

The restriction of Eq. (79) to diffusion theory and azimuthally symmetric illumination highlights the difficulty of obtaining general results in 3D radiative transfer. However, the observed violations in the ordering in Eq. (79) are not incompatible with the idea of radiative channeling picture introduced in Sec. VI.C, on the contrary. To see this, imagine, for simplicity, an isolated cloud of finite size embedded in an otherwise homogeneous optically thin atmosphere. Now, if that cloud—a strongly positive fluctuation in $\sigma(\boldsymbol{x})$—is illuminated at a grazing angle, then the sunlight is channeled upward into reflectance, as well as downward into transmittance, as defined by the local zenith. Compare Fig. 5, a schematic illustration of these $\mu_0 < 1$ effects, and Figs. 1d and 4,

[d] To model specific μ_0 effects in diffusion theory, one must separate the direct and diffuse components of radiance and write the diffusion PDE for the latter with homogeneous BCs in z and with an internal source term dependent on μ_0.

where the channeling patterns are symmetric with respect to the vertical axis. In summary, Eq. (75) shows that if $\mu_0 = 1$, then channeling contributes only to transmittance (reduces albedo) on average; this is no longer the case if $\mu_0 < 1$.

It is now easy to see why the non-IPA (channeling-driven) component of albedo reduction is of second order (hence quite small) under quasi-normal illumination at large scales: Eq. (75) is not robust with respect to deviation from $\mu_0 = 1$. On the other hand, the well-documented[38,43,51,57] break-down of the IPA at small scales is traceable, by virtue of the definitions used here, to localized channeling events under any sun angle.

VI.E. Criterion for the Onset of Strong Channeling

Whether through fully diffusive transport (as described here) or via just a couple of scatterings in an RTE-based approach,[58,59] channeling is ubiquitous because it is a symmetry-reducing (entropy-increasing) process. Since channeling occurs to some extent as soon as there is any degree of 3D variability, it is desirable to have a criterion for the onset of strong channeling. This is not hard to establish because the variability itself gives us a local length scale to compare with the local mfp $\sigma(\boldsymbol{x})^{-1}$, namely, $\sigma(\boldsymbol{x})/\|\nabla_\perp \sigma\|$. This is the nominal distance needed for $\sigma(\boldsymbol{x})$ to change by once its own value in a displacement along the direction of $\nabla_\perp \sigma$, which denotes the horizontal gradient of σ. More precisely, we are interested in the gradient perpendicular to the mean photon flow through the system, hence the subscript $\perp$ for the gradient operator. Bearing in mind that $1/\sigma(\boldsymbol{x})$ must also be on average small with respect to the outer dimensions of the system (H and L) to enable the multiple scattering, the relevant ratio is therefore

$$\zeta(\boldsymbol{x}) = \frac{\sigma(\boldsymbol{x})^{-1}}{\sigma(\boldsymbol{x})/\|\nabla_\perp \sigma\|} = \left\| \nabla_\perp \left(\frac{1}{\sigma} \right) \right\| \quad . \tag{80}$$

So we are looking at the norm of the gradient of local mfp, transverse to the mean photon flow. We will distinguish three regimes for $\zeta(\boldsymbol{x})$ where we anticipate different radiative behaviors:

1. $\zeta(\boldsymbol{x}) \ll 1$: "slow" variability. The IPA, possibly even WPP, theories will become more and more accurate.

2. $\zeta(\boldsymbol{x}) \sim 1$: "just right" variability. If persistent enough to see $\sigma(\boldsymbol{x})$ change significantly, strong channeling is likely to occur.

3. $\zeta(\boldsymbol{x}) \gg 1$: "fast" variability. If persistent over large areas, HPP theory (for mean extinction $\bar{\sigma}$) applies because almost every free path samples almost all the variability.

The first and last diagnostics are consistent with the asymptotic predictions of stochastic radiative transfer in binary mixtures,[60–63] respectively, in the limits of large and small correlation scale (the parameter of the model that controls how quickly one goes from a cloudy to a clear element or vice versa). A caveat about the second item is warranted by our discussion of Fig. 5: Because of slant illumination, channeling can have little effect on the domain average but huge effects on pixel values. For normal illumination, however, pixel-scale effects are less spectacular, but there is a definite signature of channeling in the domain average [see Eq. (75)].

To illustrate of the relevance of the nondimensional quantity in Eq. (80), we can invoke once more the sine-wave cloud model in Eq. (27) and Fig. 1. First, we note that the variability scale L has no influence on the IPA response plotted in Fig. 3b. It is however paramount to the channeling. Indeed, we have $\zeta(x) = (2\pi/L)\delta\sigma_{\max}|\sin(2\pi x/L)|/[\bar{\sigma} - \delta\sigma_{\max}\cos(2\pi/L)]^2$ from Eq. (80). Averaging over the interval $[0, L]$, we find $\bar{\zeta} = (4/\tau_{\text{hor}})\upsilon/(1-\upsilon^2)$ where $\upsilon = \delta\sigma_{\max}/(\bar{\sigma})$ is the variability parameter and $\tau_{\text{hor}} = \bar{\sigma}L$ is the horizontal optical thickness of the basic cloud cell. This average is divergent in the interesting (strong variability) limit $\upsilon \to 1^-$ because of the large and slowly changing values of $1/\sigma(x)$ at $x \approx 0$. As a characteristic value, we can, however, take

$$\zeta(L/4) = \left| \frac{\mathrm{d}}{\mathrm{d}x}\left(\frac{1}{\sigma}\right)\right|_{x=L/4} = 2\pi \frac{\delta\sigma_{\max}}{\bar{\sigma}}/\bar{\sigma}L$$

$$= 2\pi \frac{\upsilon}{\tau_{\text{hor}}} \quad . \tag{81}$$

In the numerator, the variability parameter υ cannot exceed unity in this model, so the full range of $\zeta(L/4)$ is controlled by τ_{hor} in the denominator. Equivalently, we can use the cloud's aspect ratio L/H to set the value of $\zeta(L/4) = 2\pi(H/L)\upsilon/(\bar{\tau})$. The thinner is the cell horizontally, the more values of $\sigma(x)$ each photon samples (allowed by the numerator) and the stronger are the channeling (non-IPA) effects, but only up to a point. Extinction $\sigma(x)$ can vary so fast that most photons traveling horizontally go through several cells; this happens when $\tau_{\text{hor}} = \bar{\tau}(L/H) \ll 1$, and we might as well be in a homogeneous medium with the mean extinction $\bar{\sigma}$. Table I displays Monte Carlo results for cloud transmission T with $\bar{\tau} = 15$, $\upsilon = 1$, $\mu_0 = 1$, and a wide range of L/H ratios. As predicted, T is maximum when $\zeta(L/4)$ in Eq. (81) is $O(1)$; also as predicted, $T - T_{\text{IPA}} \leq 0.02$ is not large compared to[e] $T_{\text{IPA}} - T_{\text{HPP}} \approx 0.09$. Previous numerical computations for sine-wave media using

[e] This jump is dominated by the strong direct transmission (T_{dir}) effect at $\mu_0 = 1$ in the IPA traceable to the exact alignment of the fluctuations in $\tau(x)$ and the normal illumination. Indeed, T_{dir} goes straight from $\exp(-15) \approx 3.10^{-7}$ in the HPP model at $\upsilon = 0$ (formally also $L \to 0$) to $\exp(-15)I_0(15) = 0.1039\ldots$ for any 3D model ($L > 0$) with $\upsilon = 1$; $I_n(\cdot)$ is the modified Bessel function of order n (see Sec. V.C).

TABLE I

Onset of Strong Radiative Channeling at Moderate Values of ξ in Sine-Wave Cloud Models

L/H (numeric value)[a]	$\zeta \approx 0.4 \times H/L$[b]	T (error $\times 10^3$)[c]
0/15:	∞ (HPP limit)	0.4604 (1.8)
0.1/15: (0.0067)	60	0.5440 (1.8)
1/15: (0.0667)	6.0	0.5544 (1.6)
3/15: (0.2000)	2.0	0.5623 (1.4)
10/15: (0.6667)	0.6	0.5736 (1.7)
30/15: (2.0000)	0.2	0.5710 (1.5)
100/15: (6.6667)	0.06	0.5576 (1.9)
1000/15: (66.667)	0.006	0.5539 (1.8)
∞/15:	0 (IPA limit)	0.5524 (1.3)

[a]The aspect ratio L/H of the (L-periodic) cloud model; the ratio is first stated in optical units, where $\bar{\tau}$ is held constant at 15 and τ_{hor} varies from 0 to ∞, then its numerical value is quoted.

[b]Corresponding ζ from Eq. (81).

[c]Transmission T computed with a straightforward Monte Carlo method using the maximum cross-section technique[64]; the error on T is quoted for the 10^5-history runs. For the large jump in T between $L = 0$ (formally) and $L > 0$, see Eq. (58) for the direct component.

diffusion theory[6] or the RTE (Refs. 65 and 66) confirm the aforementioned analysis.

VII. CHARACTERISTIC TIME AND LENGTH SCALES FOR DIFFUSIVE TRANSPORT IN SLAB GEOMETRY

In this section, we restore the possibility of time dependence in the RTE and in 3D diffusion to consider nonconstant and/or nonuniform sources, mostly in homogeneous media. This enables us to obtain analytical estimates of characteristic time and length scales for normal and transverse transport phenomena in finite slabs. We then confront these results with numerics for homogeneous as well as variable cloud models.

VII.A. Mean Dwelling Time

Consider a general time-dependent radiative transfer problem governed by the RTE in Eq. (1), hence the radiant energy conservation law in Eq. (11). We only require that the source have a finite duration in time, starting no sooner than $t = 0$. We can thus define

$$\langle t_{\text{inject}} \rangle = \int_0^\infty t \int_{\text{M}} S(t, \boldsymbol{x})\, \mathrm{d}\boldsymbol{x}\mathrm{d}t \Big/ \int_0^\infty \int_{\text{M}} S(t, \boldsymbol{x})\, \mathrm{d}\boldsymbol{x}\mathrm{d}t \ . \tag{82}$$

The instantaneous rate of radiant energy release by all parts of the medium's boundary ∂M (luminosity in the astrophysical literature) is defined as

$$L(t) = \int_{\partial \text{M}} \boldsymbol{n}(\boldsymbol{x}) \cdot \boldsymbol{F}(t, \boldsymbol{x})\, \mathrm{d}\boldsymbol{x} = \int_{\text{M}} \nabla \cdot \boldsymbol{F}(t, \boldsymbol{x})\, \mathrm{d}\boldsymbol{x} \ . \tag{83}$$

We can now define the mean escape time as

$$\langle t_{\text{escape}} \rangle = \int_0^\infty tL(t)\, \mathrm{d}t \Big/ \int_0^\infty L(t)\, \mathrm{d}t \ , \tag{84}$$

assuming there is no absorption in the medium, i.e., $\varpi_0 = 1$ and $\sigma_{\text{a}}(\boldsymbol{x}) = 0$ in Eq. (11). Using the remaining terms in Eq. (11) to express the integrands in Eq. (84), we have

$$\int_0^\infty L(t)\, \mathrm{d}t = \int_0^\infty \int_{\text{M}} S(t, \boldsymbol{x})\, \mathrm{d}\boldsymbol{x}\mathrm{d}t - \frac{1}{c} \left[\int_{\text{M}} J(t, \boldsymbol{x})\, \mathrm{d}\boldsymbol{x} \right]_{t=0}^{t=\infty} , \tag{85}$$

and similarly,

$$\int_0^\infty tL(t)\, \mathrm{d}t = \int_0^{\infty t} \int_{\text{M}} S(t, \boldsymbol{x})\, \mathrm{d}\boldsymbol{x}\mathrm{d}t + \frac{1}{c} \int_0^\infty \int_{\text{M}} J(t, \boldsymbol{x})\, \mathrm{d}\boldsymbol{x}\mathrm{d}t - \frac{1}{c} \left[t \int_{\text{M}} J(t, \boldsymbol{x})\, \mathrm{d}\boldsymbol{x} \right]_{t=0}^{t=\infty} , \tag{86}$$

where an integration by parts in time was applied to the term in $t\partial J/\partial t$. Since the source term is of finite duration, we have $J(0, \boldsymbol{x}) = J(\infty, \boldsymbol{x}) \equiv 0$, so the last terms in Eqs. (85) and (86) vanish identically. By substitution into Eqs. (83) and (84), we find that the mean photon path length from injection to escape is

$$\langle \lambda \rangle = c[\langle t_{\text{escape}} \rangle - \langle t_{\text{inject}} \rangle] = \int_0^\infty \int_{\text{M}} J(t, \boldsymbol{x})\, \mathrm{d}\boldsymbol{x}\mathrm{d}t \Big/ \int_0^\infty \int_{\text{M}} S(t, \boldsymbol{x})\, \mathrm{d}\boldsymbol{x}\mathrm{d}t \ . \tag{87}$$

For media with absorption ($\varpi_0 < 1$, $\sigma_{\text{a}}(\boldsymbol{x}) > 0$), the interpretation of this result is that the photon statistics we use for the averaging in Eq. (87) are conditional to escape from M (i.e., before absorption occurs on the way inside of M). The unconditional mean photon lifetime would look like $\langle t_{\text{escape}} \rangle$ in Eq. (84) but based on the sum of $L(t)$ and the instantaneous rate of absorption anywhere in M:

$$A(t) = \int_{\text{M}} \sigma_{\text{a}}(\boldsymbol{x}) J(t, \boldsymbol{x})\, \mathrm{d}\boldsymbol{x} \ ; \tag{88}$$

similarly, the mean photon lifetime conditional to ending in absorption would be based on $A(t)$ alone.

VII.B. Mean Path Lengths in Steady State and Orders of Scattering in Homogeneous Media

The general time-dependent transport result in Eq. (87) has direct bearing on steady-state problems. Indeed, a photon's pathlength λ is a well-defined geometric concept even in the absence of a time-dependent source, so its mean is simply

$$\langle \lambda \rangle = \int_{\mathrm{M}} J(\boldsymbol{x})\,\mathrm{d}\boldsymbol{x} \Big/ \int_{\mathrm{M}} S(\boldsymbol{x})\,\mathrm{d}\boldsymbol{x} \ , \tag{89}$$

conditional to escape from M, absorption by the boundary ∂M, rather than absorption in M's volume.

If we are more interested in order-of-scattering statistics, then we must consider total optical path length, which, in general, is expressed as an integral over the whole trajectory:

$$\int_{\mathrm{in}}^{\mathrm{out}} \mathrm{d}\tau(s) = \int_{\mathrm{in}}^{\mathrm{out}} \sigma(\boldsymbol{x}(s))\,\mathrm{d}s \ . \tag{90}$$

Now, for each unit of optical path length, one scattering on average has occurred. So, on the condition that we make a σ-homogeneity assumption to obtain Eq. (90) from geometrical path length λ, $\sigma\lambda$ is approximately equal to the number of scatterings from start to end, if it is sufficiently large (i.e., we are in a diffusion regime). In summary, the characteristic (actually mean) number of scatterings suffered by photons in an optically thick homogeneous medium, from injection to escape, can be estimated as follows:

$$\langle n \rangle \approx \sigma \langle \lambda \rangle = \sigma \int_{\mathrm{M}} J(\boldsymbol{x})\,\mathrm{d}\boldsymbol{x} \Big/ \int_{\mathrm{M}} S(\boldsymbol{x})\,\mathrm{d}\boldsymbol{x} \ , \tag{91}$$

where the error is systematic but certainly less than 1. Recall that $\langle n \rangle$ should always be significantly larger than unity when diffusion prevails.

VII.C. Relation to Green's Functions for Slabs in the Diffusion Limit

We now apply this result to a homogeneous plane-parallel slab medium, where $S(\boldsymbol{x}) \equiv S(z)$. Using Eq. (16) with $\partial/\partial t \equiv 0$, the scalar flux function $J(z)$ satisfies the following boundary-value problem on the interval $0 < z < H$:

$$\begin{cases} D'[-(\mathrm{d}/\mathrm{d}z)^2 + 1/L_{\mathrm{d}}^2]J = S(z) \\ [1 - \chi\ell_{\mathrm{t}}\mathrm{d}/\mathrm{d}z]J|_{z=0} = [1 + \chi\ell_{\mathrm{t}}\mathrm{d}/\mathrm{d}z]J|_{z=H} = 0 \end{cases} \tag{92}$$

in the diffusion limit, i.e., using Fick's law: $F(z) = -D'\mathrm{d}J/\mathrm{d}z$, with $D' = D/c = \ell_{\mathrm{t}}/3$. The characteristic diffusion length $L_{\mathrm{d}} = \sqrt{D'/\sigma_{\mathrm{a}}}$ in Eq. (17) naturally reappears here.

If we set $S(z) = \delta(z - z^*)$, $0 < z^* < H$, then $J(z) = G(z, z^*)$ is the Green's function of the boundary-value problem in Eq. (92); the explicit expression for $0 < z < H$ is

$$G(z,z^*) = \left(\frac{3}{\xi}\right) \frac{\left[\exp\left(\dfrac{\min\{z,z^*\}}{L_{\mathrm{d}}}\right) + (\chi\xi - 1)\right]\left[\exp\left(\dfrac{-\max\{z,z^*\}}{L_{\mathrm{d}}}\right) + \exp\left(\dfrac{-H}{L_{\mathrm{d}}}\right)(\chi\xi - 1)\right]}{2 + (\chi\xi - 1)\left[\exp\left(\dfrac{-z^*}{L_{\mathrm{d}}}\right) + \exp\left(\dfrac{z^* - H}{L_{\mathrm{d}}}\right)\right]} \ , \tag{93}$$

where $\xi = \ell_{\mathrm{t}}/L_{\mathrm{d}}$ is expressed as a function of ϖ_0 and g in Eq. (19). In the case of vanishing absorption where $\sigma_{\mathrm{a}} \to 0$ (also $\varpi_0 \to 1$, $L_{\mathrm{d}} \to \infty$, and $\xi \to 0$), we find the simpler expression

$$G(z,z^*) = \left(\frac{3\chi}{2}\right) \frac{\left(1 + \dfrac{\min\{z,z^*\}}{\chi\ell_{\mathrm{t}}}\right)\left(1 + \dfrac{H - \max\{z,z^*\}}{\chi\ell_{\mathrm{t}}}\right)}{1 + H/2\chi\ell_{\mathrm{t}}} \ . \tag{94}$$

As $z^* \to H$, the δ source reaches the upper boundary, precisely where it was placed in the diffusion treatment of albedo problem in Sec. IV.B. So one would expect $G(z,H)$ to become identical to the $J(z)$ previously obtained in Eq. (47), but we obtain a numerical factor $3\chi/2$ here, which deviates from unity if $\chi \neq 2/3$. The 3χ numerator has the same value and origin as the $|F_z|/T_{\mathrm{HPP}}$ ratio found in Sec. IV.A: We do not require Fick's law to apply strictly at the boundaries (which would otherwise enforce $\chi = 1/3$). The 2 in the denominator results from the loss of half of the strength of source inside the medium: Only the half of the isotropic energy release going downward (into the medium) is accounted for.

We can now estimate the average number of scatterings from Eq. (91), where, in this case of a δ-function source,

$$\langle n \rangle \approx \sigma \int_0^H G(z,z^*)\,\mathrm{d}z \ , \tag{95}$$

because the denominator is unity (and 1/2 if $z^* = 0, H$). Ultimately, $\langle n \rangle$ depends on all the nondimensional parameters of the problem: ϖ_0, g, $\tau = \sigma H$, and $0 \le z^*/H \le 1$.

VII.D. Extension to Horizontal Photon Transport

The characteristic order of scattering (equivalently, time scale) in Eq. (95) can be mapped to a characteristic spatial scale that describes the area of the slab-cloud that is explored by photons during their diffusive random walks, from injection to escape. To this effect, we use Einstein's relation for Brownian motion:

$$\langle \boldsymbol{r}^2(t) \rangle = Dt \ , \tag{96}$$

where $\boldsymbol{r}(t)$ is the random vector position of the particle at time t after leaving the origin at $t = 0$, and the constant $D = c\ell_t/3$ is diffusivity. Time is now mapped to the number of scatterings at escape by

$$ct \approx \langle \lambda \rangle \approx \ell \langle n \rangle = \langle n \rangle / \sigma \ . \tag{97}$$

The trick used here is that a deterministic parameter $t \ge 0$ is replaced with the average of a nonnegative random variable $\langle \lambda \rangle / c$. (The determined quantity in these truncated random walks is actually $z(t) = 0$ or H, where escape from the slab occurs.) The implicit assumption is that the pdf over which the average is performed is narrow enough to be represented by the mean alone. An important caveat about this assumption relating to reflected light was recently uncovered by Davis[67]: The pdf of n is too broad and skewed to make predictions of the higher moments from the mean alone (details to be discussed shortly).

Finally, we are interested here in the variance $\langle \rho^2 \rangle$ of the (x, y) projection of the (statistically isotropic) displacement $\boldsymbol{r}$ in 3D space. An estimate of $\langle \rho^2 \rangle$ using Eq. (96) is $\langle x^2 \rangle + \langle y^2 \rangle = (2/3)\langle \boldsymbol{r}^2 \rangle = (2/3)Dt$, which, using Eq. (14) for D, leads to $\langle \rho^2 \rangle / \langle n \rangle \approx (2/9)\ell_t/\sigma$. This, however, is certainly an underestimate because Einstein's law is strictly valid only in a boundless domain, so many events with $z > H$ or $z < 0$ are used that should not have entered the average of ρ^2, and many of those have ρ values much smaller than for a typical escape from the optically thick z-bounded medium. A somewhat better estimate is obtained by using Einstein's law in 2D, $\langle \rho^2(t) \rangle = D_2 t$, where 2D diffusivity is $D_2 = c\ell_t/2$. In summary, we have

$$\frac{\langle \rho^2 \rangle}{\langle n \rangle} \approx \frac{\ell_t}{2\sigma} = \frac{1}{2(1 - \varpi_0 g)\sigma^2} \ , \tag{98}$$

where one can use $\sigma = \tau/H$ to introduce the macroscopic cloud properties as needed. However, a unified time-space theory of photon diffusion in vertically finite media with the appropriate BCs and initial condition for a pulsed point source on a boundary (hence no need to invoke Einstein's law) has been developed[f] by Davis et al.[15] Their computations are restricted to the case of reflection with $\varpi_0 = 1$, but that does not affect their independent estimate of $\langle \rho^2 \rangle_R / \langle n \rangle_R = (4/3)\ell_t/\sigma$, which is more than twice as large as in Eq. (98). This discrepancy is probably caused by the broadness and skewness of the pdf in n for reflection.

The square root of $\langle \rho^2 \rangle$ is the characteristic root-mean-square (rms) horizontal transport scale; it will depend on all the nondimensional quantities in $\langle n \rangle$ from Eq. (95), plus a length-scale (e.g., ℓ_t or H). Physically, $\langle \rho^2 \rangle^{1/2}$ measures the (gyration) radius of the combined time-integrated spots of light at the two boundaries, assuming a δ function for the spatial pattern of the source in (x, y) as well as in z.

VII.E. $\langle n \rangle_F$ (F = R,T) and Horizontal Transport Scales for Slab Geometry: Conservative Case

By substitution of Eq. (94) into Eq. (95), we obtain

$$\langle n \rangle \approx \frac{3\chi}{2} \sigma H \left[1 + \left(\frac{z^*}{H} \left(1 - \frac{z^*}{H} \right) \right) \frac{H}{\chi \ell_t} \right] \ . \tag{99}$$

Recalling that $\sigma H = \tau$ (optical thickness of the slab) and that $\ell_t = [(1 - g)\sigma]^{-1}$, we have

$$\langle n \rangle (1, g, \tau; z^*/H) \approx \frac{3\chi}{2} \tau \left[1 + \left(\frac{z^*}{H} \left(1 - \frac{z^*}{H} \right) \right) \frac{(1 - g)\tau}{\chi} \right] \ . \tag{100}$$

For a source deep inside the medium (and, by association, transmitted photons), we obtain

$$\langle n \rangle_T (1, g, \tau) \approx \frac{3}{8} (1 - g)\tau^2 + \frac{3\chi}{2} \tau \tag{101}$$

by setting $z^* = H/2$ in Eq. (100) for specificity. As expected, we find that $\langle n \rangle_T$ becomes $\propto (1 - g)\tau^2$ asymptotically, i.e., when $(1 - g)\tau \gg 4\chi$, and this is independent of χ (i.e., BC details). We use here the subscript T to designate transmission even though the source is at the center plane of the slab.

The quadratic term in Eq. (101) vanishes identically if the source is moved to a boundary ($z^* = 0$ or H); we are then left with

$$\langle n \rangle_R (1, g, \tau) \approx 3\chi\tau \ , \tag{102}$$

[f]These authors are motivated by the idea of using a pulsed laser to measure $\langle \lambda \rangle$ (based on time) and $\langle \rho^2 \rangle$ (based on imaging) to infer the fundamental geometric and optical cloud properties, namely, H and τ (or σ), by active remote sensing (this implies that only reflected radiances can be used). Reasons why this is possible will soon become clear. Time-dependent diffusion theory plays a central role here, but the signals of interest are not affected by its shortcomings at early times and small distances from the laser beam.

remembering to first multiply the result in Eq. (95) by 2 to account for the loss of source strength in the limit $z^* \to 0, H$. That $\langle n \rangle_R$ is $\propto \tau$ is also a well-known fact in radiative transfer theory; we note here that this proportionality law does not depend on g (i.e., scattering details). Although escapes from both boundaries are considered here together, clearly, the low n values coming from the same boundary as where the source is placed dominate in Eq. (102). This is a characteristic of reflected fluxes, hence the subscript R. The more detailed calculation in reflectance mentioned previously[15] is based on a closed-form solution in Laplace space. It yields $\langle \lambda \rangle_R / H \approx \langle n \rangle_R / \tau \to 2\chi$ as $\tau \to \infty$ with a pre-asymptotic correction term $[1 + (\epsilon/2)(1 + 3\epsilon/2)/(1 + \epsilon)] \geq 1$ in the small parameter $\epsilon = 2\chi/(1 - g)\tau = T/R$; this correction is not small at typical cloud optical depths: When $\epsilon = 2/3$ ($\tau \approx 30$ if $g \approx 0.85$, $\chi \approx 2/3$), it is still $7/5 = 1.4$, and this is in the direction that makes Eq. (102) look more accurate than $2\chi\tau$ at these intermediate τ values.

Time-domain results similar to Eqs. (101) and (102) follow from asymptotic radiative transfer theory, but their derivation[27] in that framework is not as simple to follow as here. We have already mentioned that they are well-known in the sense of the exponents of τ, but the prefactors (and what they depend on) are not usually stated. It is sometimes overlooked that it is not the number of scatterings that is linear or quadratic in τ but its mean, at best a typical value. In fact, Davis[67] showed recently with simple scaling arguments that Eq. (102) will be a poor predictor for the rms order of scattering $\langle n^2 \rangle_R^{1/2}$ because the pdf of pathlength λ (hence n) in reflection is actually quite broad. Specifically, one finds[15]

$$\frac{\langle n^2 \rangle_R}{\langle n \rangle_R^2}(1, g, \tau) \approx \frac{\langle \lambda^2 \rangle_R}{\langle \lambda \rangle_R^2}(1, g, \tau) \approx \frac{(1 - g)\tau}{5\chi} \qquad (103)$$

for asymptotically large τ. However, this does not deter us from using $\langle n \rangle_R$ as a characteristic number of scatterings in the following, largely because the ratio in Eq. (103) remains $O(1)$ until τ significantly exceeds $5\chi/(1 - g) \approx 24$ under normal conditions in clouds ($g \approx 0.85$, $\chi \approx 0.71$).

Using Eqs. (98) and (101), we obtain the variance of the horizontal displacement for transmittance:

$$\langle \rho^2 \rangle_T(1, g, \tau, H) \approx \frac{3}{16} H^2 + \frac{3\chi}{4} \ell_t H \ , \qquad (104)$$

where the second term becomes negligible when $\ell_t \ll H$, or $(1 - g)\tau \gg 1$. So $\langle \rho^2 \rangle_T \propto H^2$, independently of τ, χ, and g. This is almost what we expect intuitively since we can visualize a spherical diffusive wave of photons emanating from a point at the center ($x = y = 0, z = H/2$) of the optically thick slab; when intercepted at the boundaries ($z = 0, H$), its radius is $H/2$, which is very close to $\sqrt{\langle \rho^2 \rangle_T}$ in Eq. (104).

For reflectance, Eqs. (98) and (102) yield

$$\langle \rho^2 \rangle_R(1, g, \tau, H) \approx \frac{3\chi}{2} \ell_t H = \frac{3\chi}{2} \frac{H^2}{(1 - g)\tau} \ . \qquad (105)$$

The more detailed calculation for reflectance by Davis et al.[15], this time in Fourier space, again yields a different asymptotic prefactor: $(1 - g)\tau \times \langle \rho^2 \rangle_R / H^2 \to 8\chi/3$ as $\tau \to \infty$ and the same pre-asymptotic correction term as for $\langle \lambda \rangle_R / H \approx \langle n \rangle_R / \tau$. At any rate, $\sqrt{\langle \rho^2 \rangle_R}$ decreases quite slowly as τ increases, in $1/\tau^{1/2}$ for a given H. This is enough, however, to make it smaller than $\sqrt{\langle \rho^2 \rangle_T}$, which is asymptotically independent of τ. In turn, this is why the endpoints of the flux lines in Fig. 1d are anticipated to be more evenly spread out than their departure points.

The spatial counterparts of Eqs. (101) and (102), in Eqs. (104) and (105), respectively, for horizontal—generally speaking, transverse—particle displacement have not received much attention in the literature. Notable exceptions are the independent studies by Reynolds, Johnson, and Ishimaru[68] and Weinman and Masutani,[13] respectively, on medical and atmospheric issues. However, it is noteworthy that simultaneous measurements of $\langle \lambda \rangle_R$ and $\langle \rho^2 \rangle_R$ can be used to infer H and $(1 - g)\tau$, and $\sigma = \tau/H$ from there. Moreover, this can in principle be done remotely for clouds using a lidar system with imaging capability and a wide enough field of view. This application, and others discussed in Sec. VIII, are bringing Eqs. (104) and (105) into the limelight, at least in atmospheric radiation.

VII.F $\langle n \rangle_R$ and the Related Horizontal Transport Scale in Slab Geometry: Absorbing Cases

We will consider only reflection, so we set $z^* = 0$ or H in Eq. (93) and then substitute the result into Eq. (95), with the appropriate multiplication by 2. We find

$$\langle n \rangle_R(\varpi_0, g, \tau) \approx \left(\frac{3\chi}{\kappa} \right) \frac{[1 - \exp(-\kappa\tau)] + \kappa\tau(\xi\chi - 1)\exp(-\kappa\tau)}{1 + (\xi\chi - 1)[1 + \exp(-\kappa\tau)]/2} \ , \qquad (106)$$

where $\kappa = \kappa(\varpi_0, g) = 1/\sigma L_d$ and $\xi = \xi(\varpi_0, g)$, as defined in Eqs. (18) and (19), respectively. This generalizes Eq. (102) for $\varpi_0 < 1$, noting, however, that retrieving Eq. (102) from Eq. (106) in the limit $\varpi_0 \to 1$ ($\kappa \to 0$) at fixed τ, calls for a second-order expansion of the exponentials in $\kappa\tau$ then application of l'Hôpital's rule.

Instead of increasing linearly with τ indefinitely, $\langle n \rangle_R(\varpi_0, g, \tau)$ now crosses over to a flat asymptote at

$$\langle n \rangle_R(\varpi_0, g, \infty) \approx \frac{6\chi}{\kappa[1 + \chi\xi]} \ , \qquad (107)$$

when $\tau > 1/\kappa$. In the limit $\varpi_0 \to 1$ ($\xi \to 0$) and for very large τ, we therefore have

$$\langle n\rangle_{\mathrm{R}}(\varpi_0, g, \infty) \approx \frac{6\chi}{\kappa} \approx 2\chi\left(\frac{3}{1-g}\right)^{1/2}(1-\varpi_0)^{-1/2} \quad . \quad (108)$$

At such large optical thicknesses, everything happens physically as if there were no absorption but the geometric thickness H of the medium was equated with L_{d}; equivalently, $1/\kappa$ was its optical thickness τ in Eq. (102).

As in Sec. VII.E, we can derive from Eq. (98) the variance in horizontal displacement for reflected photons:

$$\langle \rho^2\rangle_{\mathrm{R}}(\varpi_0, g, \tau, H) \approx \left(\frac{\langle n\rangle_{\mathrm{R}}}{2(1-\varpi_0 g)\tau^2}\right)H^2 \quad . \quad (109)$$

Because the numerator ceases to increase with τ for $\tau > 1/\kappa$, the behavior of $\sqrt{\langle \rho^2\rangle_{\mathrm{R}}}$ changes from $H/\tau^{1/2}$ to a steeper decrease in H/τ, for given g and ϖ_0. Even more importantly, $\sqrt{\langle \rho^2\rangle_{\mathrm{R}}}$ is a strong function of $1-\varpi_0$, which varies far more than g in clouds (with wavelength across the solar spectrum). Indeed, we see that in the limit $\varpi_0 \to 1$, Eqs. (108) and (109) yield

$$\sqrt{\langle \rho^2\rangle_{\mathrm{R}}}(\varpi_0, g, \tau, H) \approx 3^{1/4}\chi^{1/2}(1-g)^{1/4}(1-\varpi_0)^{-1/4}\frac{H}{\tau} \quad (110)$$

as long as $\tau > 1/\kappa$, which is itself increasing as $\varpi_0 \to 1$.

In contrast with the relatively simple mathematics of diffusion theory leading to an approximate but closed-form result for $\langle n\rangle_{\mathrm{R}}$ in Eq. (106), Platnick[69] uses a sophisticated adding-and-doubling technique to obtain accurate numerical estimates of $\langle n\rangle_{\mathrm{R}}$, $\langle n\rangle_{\mathrm{T}}$, and even the internal profiles of mean order of scattering in both directions. His follow-on study[70] of horizontal displacement focuses on $\sigma^2\langle \rho^2\rangle_{\mathrm{R}}$, which according to Eq. (98), is proportional to $\langle n\rangle_{\mathrm{R}}/(1-\varpi_0 g)$; being a distance reckoned in optical units, it is a function only of the nondimensional parameters (ϖ_0, g, τ) and H is never considered explicitly.

VII.G. Comparison of Diffusion Predictions with Numerical RTE Solutions, and 3D Effects

Figure 6 shows $\langle n\rangle_{\mathrm{R}}(\varpi_0, g, \tau)$ as a function of τ for g = 0.85 and selected values of ϖ_0: 0.999, 0.99, 0.95, and 0.9. The formula in Eq. (106) with $\chi \approx 0.5$ follows quite closely the numerical results obtained by Monte Carlo solution of the RTE, at least at optical thickness large enough ($\tau \gtrsim 10$) for the diffusion model to apply. This is true at all the levels of absorption considered. The particular value selected for the $O(1)$ extrapolation length constant χ in the BCs in Eq. (31) was determined by trial

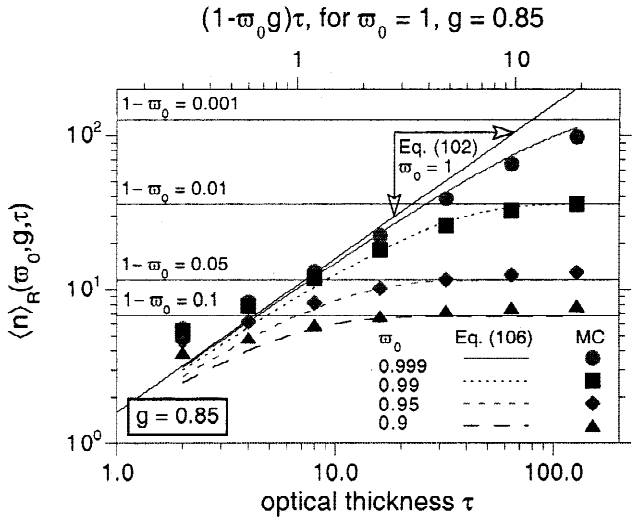

Fig. 6. Mean number of scatterings in light reflected from homogeneous scattering and absorbing slabs. We compare the predictions of diffusion/P_1 theory (lines and curves) with results of a numerical solution of the RTE (symbols). The latter were obtained from Monte Carlo simulations for diffusely illuminated homogeneous plane-parallel media with seven optical depths from 2 to 128, by powers of 2, and a Henyey-Greenstein phase function with $g = 0.85$. The absorption parameter $1-\varpi_0$ ranges from small (but nonnegligible at large τ) to the point where diffusion theory is expected to fail according to Eq. (24) when $g = 0.85$. We used $\chi \approx 0.5$ in Eq. (106) to fit the numerical data in the diffusion regime ($\tau \gtrsim 10$).

and error and is clearly determined in large part by the 3χ factor in Eqs. (102) and (106). We recall that the different implementation of the diffusion model by Davis et al.[15] for $\varpi_0 = 1$ in plane-parallel media leads instead to a factor of 2χ in Eq. (102); in that version of the model (not yet extended to $\varpi_0 < 1$ cases), we would likely find $\chi \approx 0.75$ more suitable than unity, and closer to the canonical values of 2/3 and 0.7104… in Eq. (32)

Figure 7a shows our diffusion-based prediction for the dependence on τ of the rms horizontal displacement in Eq. (109) using Eq. (102) or Eq. (106), respectively, for $\varpi_0 = 1$ and $\varpi_0 = 0.99$, 0.95, or 0.90. The analytical results again compare well with the corresponding RTE results for homogenous cloud models using $\chi \approx 1.1$ this time; again, a more accurate estimate of the prefactor in Eq. (98), hence in Eq. (106), would bring the effective χ down by at least half of this value, hence quite close to the standard choices. Figure 7b is for random fractal cloud models, which are described in more detail in the next section (see Fig. 8). In this case, the abscissa is the mean optical depth, and the RTE solutions are averaged over all possible source positions and a few realizations of the disorder. We see that the agreement would still be acceptable for $\varpi_0 = 1$ (no absorption) as long as the prefactor is further increased. However, we can also see that the performance of the theory deteriorates rapidly as ϖ_0

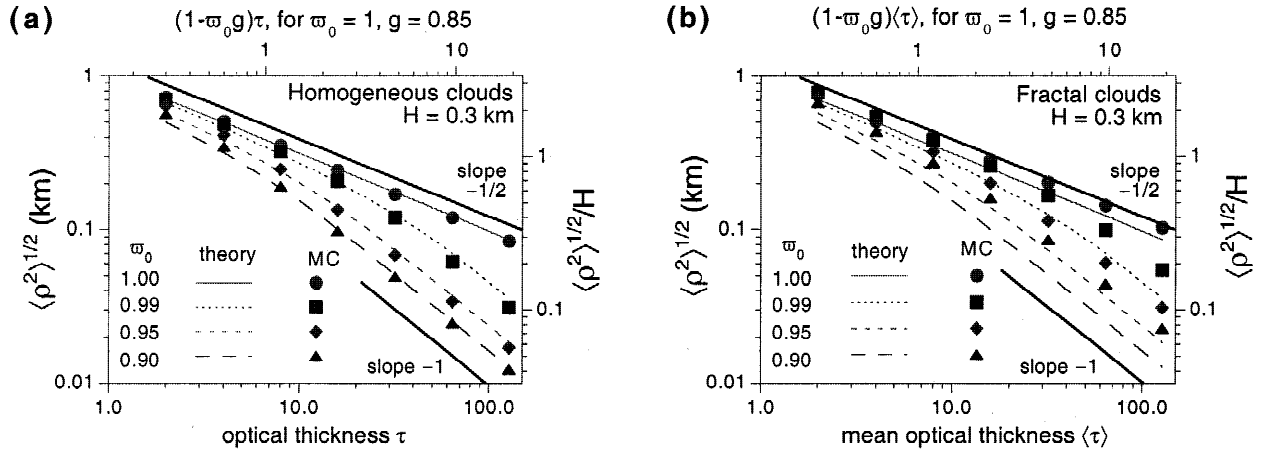

Fig. 7. The RMS horizontal (transverse) displacement of light reflected from scattering and absorbing slabs. The point source at the upper boundary is isotropic. Four single-scattering albedoes ϖ_0 are used: 1.00, 0.99, 0.95, and 0.90. The optical depth sequence and phase function are the same as in Fig. 6; the reference lines are $\propto\tau^{-1/2}$, corresponding to $\varpi_0 = 1$ in Eq. (105) and $\propto\tau^{-1}$ for $\varpi_0 < 1$ and $\tau\kappa \gg 1$ in Eq. (110). (a) Homogeneous plane-parallel media with $H = 0.3$ km. As in Fig. 6, fitting of the Monte Carlo data using the numerical extrapolation-length constant leads here to $\chi \approx 1.1$ (further discussion in main text). (b) Same outer geometry and optical properties as in Fig. 7a but extinction is horizontally variable, as described in Sec. VIII and Fig. 8; in this case, the point sources are uniformly distributed over the upper boundary. The analytical diffusion theory is unmodified from Fig. 7a, and the resulting discrepancies are discussed in the text.

decreases (absorption increases). We note that the sign of the deviation of fractal numerical results with respect to their homogeneous analytical counterparts is consistent with Jensen's inequality if $\sqrt{\langle\rho^2\rangle_R}(\varpi_0, g, \tau, H)$ is treated similarly to $T(\mu_0, \varpi_0, g, \tau)$ in Sec. V.C. Furthermore, the deviation is small for $\varpi_0 = 1$ because the τ dependence is nonlinear but relatively weak ($\sim 1/\tau^{1/2}$), and it is large for $\varpi_0 < 1$, especially at large τ values where the nonlinearity of $\sqrt{\langle\rho^2\rangle_R}$ is stronger ($\sim 1/\tau$).

VIII. RADIATIVE SMOOTHING: THEORY, VALIDATION, AND APPLICATION TO BREAKDOWN OF INDEPENDENT PIXEL APPROXIMATION

Section VII was concerned mostly with time-domain computations in homogeneous uniformly illuminated plane-parallel media and the spatial ramifications for a δ-function illumination pattern. We now return to genuine 3D radiative transfer properly equipped to discuss the practical limitations of the widely used IPA, which, we recall, has a tremendous computational advantage over any implementation of 3D radiative transfer, even in the diffusion limit.

Several studies (e.g., Refs. 53, 71, and 72) have compared IPA and exact RTE solutions for domain averages. Considering the variable area-averaged quantities in Eqs. (37), (38), and (39), the lower bound on the averaging scale r at which the IPA can be used must satisfy $\bar{\Delta}(r, \cdot) \approx 0$ using the notation from Eq. (39). An a priori

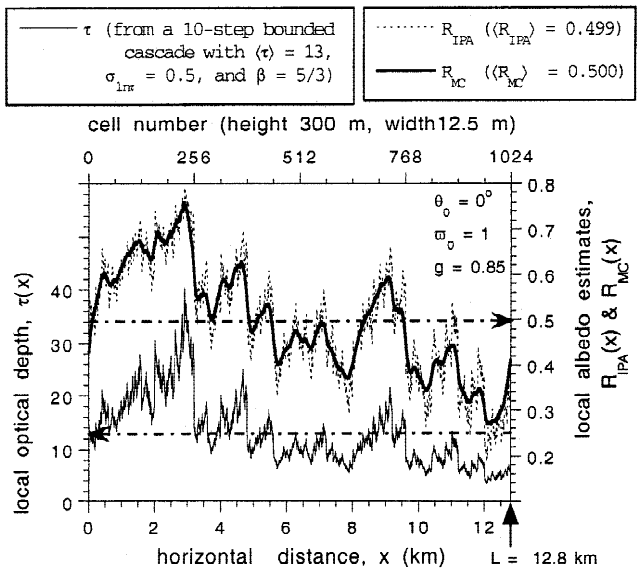

Fig. 8. Fractal cloud model and associated radiation fields. The lower plot and left axis are for the horizontal profile of optical depth through cloud $\tau(x)$ that was generated using a bounded cascade.[74] Geometrically, the cloud is plane-parallel with thickness $H = 0.3$ km; by construction (ten cascade steps), it is made of $2^{10} = 1024$ cells, each 12.5 m wide (aspect ratio $12.5/300 = 1/24$). For the radiative transfer, scattering is conservative ($\varpi_0 = 1$), a Henyey-Greenstein phase function is used ($g = 0.85$), the sun is at zenith ($\mu_0 = 1$), and cyclical BCs are applied. The upper plots are of the local albedo field $R(x)$ computed with the IPA (rough dotted line) and by Monte Carlo (smooth full line). The effect of radiative smoothing (decreased variance at the small scales) is obvious in the latter.

determination of this scale in stratiform cloud types was obtained by Davis et al.[38] at conservative wavelengths by invoking the theory of radiative smoothing developed by Marshak et al.[57] In turn, the theory of radiative smoothing hinges on the rms horizontal displacements computed in Sec. VII in the diffusion limit.

The notion of radiative smoothing was in fact first described by Stephens in Ref. 55 (p. 1833): "For the case p [$\langle\tau\rangle$-doubling step] = 1 [very small $\langle\tau\rangle$], ... there is a one to one correspondence between the structure of the reflectance and the specified structure of the optical properties. As p increases [$\langle\tau\rangle$ gets large], the spectra of R falls off more and more rapidly with increasing u [wavenumber] .... These results thus suggest that multiple scattering tends to filter out the fine structure in the radiation field." However, it took almost a decade before this qualitative description was given a quantitative meaning through the work of the present authors and co-workers at the National Aeronautics and Space Administration (NASA), Goddard Space Flight Center. During this time period, the radiative properties of stratiform clouds in the marine boundary layer were systematically investigated because of their strong impact on the planetary albedo (they are highly persistent and extend over thousands of kilometres). Geometrically, these stratocumulus are almost plane-parallel, and it is tempting to model them with HPP theory. However, internally they are extremely variable,[73] and the NASA group advocated and used fractal cloud models[74] called bounded cascades to simulate the horizontal variability in optical depth. For our present purposes, it suffices to know two things about the key observations of the stratus clouds and the adopted fractal models: (a) that the one-point pdf of $\tau(x, y)$ is approximately lognormal with a mean in excess of 10 and (b) that the two-point autocorrelation properties of $\tau(x, y)$ are described by a power-law wavenumber spectrum:

$$E_\tau(k) \propto k^{-\beta} \tag{111}$$

with $\beta \approx 5/3$ (as predicted in statistical turbulence theory) for scales $r = 1/k$ ranging from at least tens of kilometres down to only a few metres (i.e., over three decades of scaling). For $\beta < 3$, graphs of $\tau(x, y)$ transects are nondifferentiable, geometrically rough sets; an example is shown in Fig. 8 (lower plot). By any account, the dimension of a smooth (differentiable) graph is 1, but the inherent dimension D_g of this graph is fractal, somewhere between 1 and 2. Mandelbrot[75] shows that D_g is given by $(5 - \beta)/2$ for $1 < \beta < 3$; this yields $D_g \approx 5/3$ for $\beta = 5/3$. Utilization of such naturally rough optical media proved essential in measuring the smoothing power of radiative transfer.

The IPA radiance fields associated with the fractal optical depth fields, computed pixel-by-pixel with a 1D model, have spectra following the same power-law (only the prefactor changes) as the optical depth. In contrast, the spectra of the numerically calculated 3D radiance fields follow a similar power law, but only down to a few hundred metres (see $\varpi_0 = 1$ case in Fig. 9). At the smallest scales, below this scale break, there is a significant deficit of variance, hence the term radiative smoothing. The special scale at which this scale break occurs [envision the intersection of two lines on a log-log plot of $E_I(k)$ versus k] is denoted η_R. Extensive numerical experimentation showed that η_R has the same dependence on H, g, and τ (equated with the domain-average value $\bar{\tau}$) as $\sqrt{\langle\rho^2\rangle_R}$ in Eq. (105). So the diffusion-based theory of horizontal photon transport in homogeneous slab clouds captures the basic phenomenology of radiative smoothing in highly variable fractal clouds. In return, the ubiquitous observation of radiative smoothing in real stratocumulus confirms the assertions by King, Radke, and Hobbs[37] about the validity of diffusion as a reasonable model for radiation transport in these dense boundary-layer clouds.

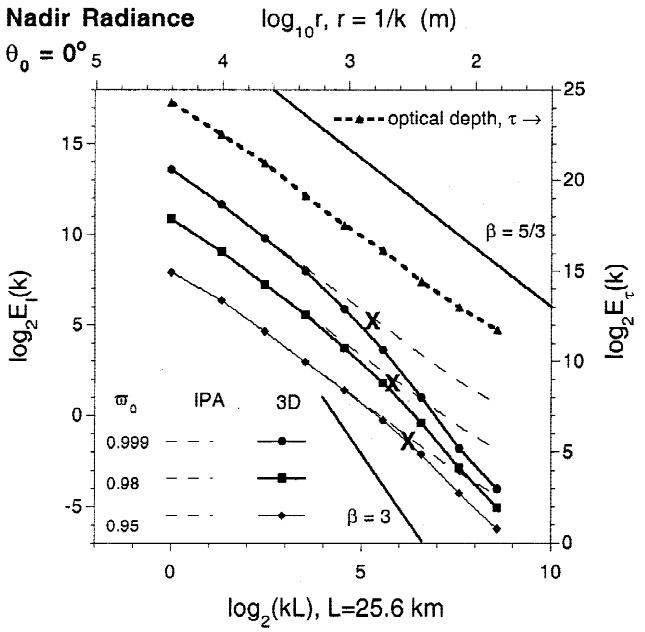

Fig. 9. Wavenumber spectra $E_\tau(k)$ and $E_I(k)$ for both IPA and 3D nadir radiance fields. As in Fig. 8, the fractal distributions of cloud optical depth (upper curve) are obtained using bounded cascades set for $\bar{\tau} = 13$, the standard deviation of $\ln\tau$ is 0.5, and $\beta = 5/3$; the variability unfolds in the x direction only. Pixel size is 25 m; cloud top and base are flat and thickness $H = 300$ m. A Henyey-Greenstein phase function with $g = 0.85$ is used and solar zenith angle θ_0 is 0 deg. Results are averaged over ten independent realizations. Three single-scattering albedoes ϖ_0 are used (0.999, 0.98, and 0.95) and Xs indicates the scale-break positions $\eta_R(\varpi_0)$.

The most important application of radiative smoothing theory is to significantly enhance our understanding of why and when the IPA breaks down: At scales below $\eta_R \sim \sqrt{\langle\rho^2\rangle_R}$, solar photons typically visit (via multiple

scattering) areas containing σ values too different to neglect 3D effects. Characterizing IPA breakdown is a critically important task because the IPA is the operational procedure in all current cloud remote sensing with satellites. The improved resolution of current and future spaceborne instruments guarantees that 3D effects are present in the radiometry and will not go away. In this remote-sensing context, a nonlocal IPA has been developed to improve the small-scale performance of the IPA without jeopardizing its computational efficiency.[76] The IPA is also used routinely in dynamical simulations on supercomputers of atmospheric processes such as cloud formation and evolution. Here again, the timeline of computer memory and speed enhancements guarantees that 3D radiative transfer effects cannot be neglected forever without introducing biases. A computationally efficient approach such as 3D photon diffusion will become necessary and desirable.

An important intermediate step in going from the analytical results for lateral diffusion in highly idealized homogeneous clouds to real clouds is to compare them with numerical simulations in the more realistic fractal cloud models, as was done in Fig. 7b. The deviations between fractal and uniform clouds observed there are large enough to motivate an in-depth study of these variability effects. This is indeed a prerequisite to make a priori prediction about the position η_R of the scale-break (i.e., where the IPA breaks down) based on the rms horizontal transport distance $\sqrt{\langle \rho^2 \rangle_R}$ in the presence of absorption. In the meantime, the energy spectra of radiance fields for $\varpi_0 = 0.98$ and 0.95 in Fig. 9 show the expected trend with respect to the conservative case: η_R decreases rapidly with ϖ_0, as does $\sqrt{\langle \rho^2 \rangle_R}$ in Eq. (110). Furthermore, the variance relative to the IPA prediction is less reduced as ϖ_0 decreases because more absorption means less scattering, hence less smoothing.

Wavenumber spectra of high-resolution cloud imagery from satellites show radiative smoothing and therefore validate empirically this piece of radiative diffusion theory.[38] More recently, Savigny et al.[77] conducted a scale-by-scale statistical study of time series of zenith radiance at ground level under heavy cloudiness; they were thus able to extend this validation from reflectance to transmittance using the dominant term in Eq. (104). Since radiative smoothing is now readily observable as a statistical signature of many internal channeling events (defined in Sec. VI in reference to the structure of photon flow beyond the IPA), we see that this bestows onto 3D atmospheric radiative transfer the status of experimental science.[78] This important milestone was reached in no small way thanks to P_1/diffusion theory. Although there are still many open questions about diffusion, channeling, radiative smoothing and net horizontal photon transport in clouds, insights have been gained on the fundamental aspects of macroscopic interaction of radiation and matter.

IX. SUMMARY, DISCUSSION, AND OUTLOOK

We have described how the relevant radiative transfer in clouds calls for multiple scattering and how this is precisely what complicates the problem as soon as one wants to model variability in more than the vertical direction. Although there are even simpler approaches to the 3D problem that provide partial answers, the diffusion equation offers more insight into the mechanisms of macroscopic radiation-matter interaction in a 3D setting than the more physically correct RTE. To wit, we derive a general 3D result that appears in Eq. (75) linking the change in domain-average flux to the covariance of fluctuations in local density and flux, assuming both mass and number of photons are conserved. Furthermore, this result illustrates the general mechanism by which radiation flows through a variable medium, namely, a radiative channeling, where the photons flow around concentrations of scattering material and into the more tenuous areas. We also used diffusion theory to estimate some characteristic temporal and spatial scales pertaining to transport through finite scattering media, with and without absorption. These scales are used to cast new light onto channeling processes in clouds as well as to find the robust statistical features of remotely sensed radiance fields where channeling manifests itself.

For almost four decades, the main motivation behind studies of 3D radiative transfer in the atmosphere was the obvious fact that real clouds are not infinite homogeneous plane-parallel slabs, and since such homogeneous plane-parallel models are the operational standard in meteorology, we need to evaluate the bias they introduce. Three-dimensional theory is thus compared to itself for validation and to 1D theory as a benchmark. Recently, this paradigm has shifted toward the confrontation of specific predictions of 3D theory against observations, e.g., the scale break in LANDSAT imagery.[38] This means that atmospheric 3D radiative transfer has matured into a stand-alone science: It has both theoretical and experimental facets and, of course, applications. For instance, we have pointed out that the space-time phenomenology of normal and transverse photon transport in slab geometry described in Sec. VII is currently receiving experimental validation. It has also inspired new cloud remote-sensing methods, both passive[76] and active.[15]

We have used diffusion theory here exclusively as a formalism that facilitates analytical investigations of steady-state 3D photon transport, as well as time-dependent 1D transport, and the problem of steady but localized sources in 1D and in 3D. However, there is more to the photon diffusion picture. The diffusion equation, being a standard in mathematical physics, can be solved numerically with extreme efficiency (by comparison with RTE solvers). This opens the door to several new applications: interactive 3D radiation transport in 3D dynamical cloud modeling and the exciting possibility

of 3D optical cloud tomography. The latter example is similar to new developments in noninvasive medical imaging through soft tissue.[79]

We have emphasized that diffusion is a self-consistent transport theory, a conceptual model where photons travel on convoluted random walks obeying Gaussian statistical laws such as Eq. (96): distance $\propto \sqrt{\text{time}}$. We have not forgotten, however, that diffusion is also just an approximation to radiative transfer; we underscored its limitations and listed ways of improving on them to some extent. As stated early in this paper, diffusion theory applies only inside the densest clouds the atmosphere offers, often residing in the lower few kilometres (the planetary boundary layer). Diffusion theory does not work at all in the quasi-optical vacuum between clouds, and not much better in the more tenuous clouds aloft (altocumulus and cirrus). That is why we have proposed[80] a modified photon diffusion theory based on Lévy-stable (rather than Gaussian) steps between scatterings to capture, in a 1D setting, some of the complexity of 3D radiative transfer through a cloudy atmospheric column. This generalization of diffusion theory, unfortunately, does not yet have a rigorous mathematical formulation, so we are left with numerical simulations (in 1D) and anomalous scaling counterparts to Eq. (96): distance $\propto \text{time}^{1/\alpha}$ $(1 < \alpha < 2)$. Using a state-of-the-art optical spectrometry to obtain high-resolution scans of the oxygen A-band, Pfeilsticker[81] recently showed that the Lévy-flight model naturally explains solar path-length observations under a wide variety of cloud covers.

We have now gone full-circle: from the deterministic treatment of the highly idealized sine-wave cloud model (used by us as well as by others to illustrate the basics of 3D radiative transfer), to the arguably more realistic fractal cloud models (treated deterministically one realization at a time before ensemble-averaging the numerical results in Fourier space), to the Lévy-flight model for whole-atmosphere photon kinetics, which is inherently stochastic (it only predicts domain-and-ensemble-average fluxes). Here is where we meet Jerry Pomraning again. Following the pioneering work of Avaste and Vainikko,[60] Jerry wrote the definitive book[82] on transport in random binary mixtures and found a natural application in broken cloudiness.[62,63] He also pushed the envelope of stochastic radiative transfer far beyond the standard assumption of two extinction values in Markovian patterns, possibly with atmospheric applications in mind.

POSTSCRIPT

'. . . life is an integral'
Jerry Pomraning

We are compelled under the present circumstances to briefly reminisce about Prof. G. C. "Jerry" Pomraning and the interest that he developed for atmospheric radiation problems, particularly with clouds, in recent years—only a few years that sadly turned out to be his last. The authors met Jerry at the Third Science Team Meeting of the U.S. Department of Energy's (DOE's) Atmospheric Radiation Measurement (ARM) Program, March 1–4, 1993, in Norman, Oklahoma, through mutual colleagues and friends. At that precise moment, this radiative transfer guru was vigorously playing ragtime strides on an old upright. Jerry had many friends—a better description than colleagues here because of his contagious conviviality—and these friends were involved in many fields of research. He encouraged his friends to explore new areas and followed his own advice to the letter and reveled in doing it. We can vividly remember this die-hard urbanite happily romping around the muddy fields of Oklahoma that had just recently been converted into an atmospheric radiation instrument park at ARM's Cloud and Radiation Testbed site. After befriending Jerry in '94, we met several times again at other atmospheric radiation meetings, at seminars he gave at our institutions, at his University of California at Los Angeles office, and at his home. Only a year ago, we were looking forward, as always, to seeing him again. Indeed, Jerry had enthusiastically agreed to give an invited talk at a special 3D atmospheric radiative transfer meeting[78] we organized in June 1999 to commemorate the career of Georgii Titov, a prominent cloud radiation expert and a very special friend of Jerry's, who had died of cancer the year before. Alas, by February Jerry had left us. . . .

Dr. Pomraning was able to convey ideas on the most arcane aspects of stochastic radiative transfer very clearly to lay audiences from the atmospheric community as he explained how the theory applies to their issues. Here, we hoped to reciprocate somehow for Jerry's native community of neutron transport theory with the 3D radiative transfer results we have presented addressing atmospheric radiation problems but using a formalism shared by neutron and photon transport theories. In fact, Jerry Pomraning read an early version[83] of Secs. II through VI and offered several constructive comments. It seemed fit to use that improved material here and blend it with more recent work.

ACKNOWLEDGMENTS

This work was supported by the Environmental Sciences Division of the DOE (under grant DE-A105-90ER61069 to NASA's Goddard Space Flight Center) as part of the ARM program. We thank N. Byrne, R. Cahalan, R. Davies, F. Evans, M. King, Y. Knyazikhin, D. Levermore, S. Lovejoy, L. Oreopoulos, K. Pfeilsticker, S. Platnick, G. Stephens, G. Titov, J. Weinman, and W. Wiscombe for many fruitful discussions. We are specially appreciative of the insightful comments given to us by the late G. C. Pomraning on an early version of Secs. II through VI of this paper.

REFERENCES

1. B. WIELICKI, B. R. BARKSTROM, E. F. HARRISON, R. B. LEE, G. L. SMITH, and J. E. COOPER, "Clouds and the Earth's Radiant Energy System (CERES): An Earth Observing System Experiment," *Bull. Am. Meteor. Soc.*, **77**, 853 (1996).

2. K.-N. LIOU and Y. TAKANO, "Light Scattering by Nonspherical Particles in Remote Sensing and Climate Applications," *J. Atmos. Sci.*, **51**, 271 (1994).

3. R. W. PREISENDORFER, *Hydrological Optics*, National Oceanic and Atmospheric Administration, PMEL, Hawaii (1976).

4. R. G. GIOVANELLI, "Radiative Transfer in Non-Uniform Media," *Aust. J. Phys.*, **12**, 164 (1959).

5. V. L. GALINSKY and V. RAMANATHAN, "3D Radiative Transfer in Weakly Inhomogeneous Media—Part 1: Diffusive Approximation," *J. Atmos. Sci*., **55**, 2946 (1998).

6. J. A. WEINMAN and P. N. SWARTZTRAUBER, "Albedo of a Striated Medium of Isotropically Scattering Particles," *J. Atmos. Sci.*, **25**, 497 (1968).

7. B. R. BARKSTROM and R. F. ARDUINI, "The Effect of Finite Size of Clouds upon the Visual Albedo of the Earth," *Radiation in the Atmosphere*, p. 188, H.-J. BOLLE, Ed., Science Press, Princeton, New Jersey (1977).

8. R. DAVIES, "The Effect of Finite Geometry on the Three-Dimensional Transfer of Solar Irradiance in Clouds," *J. Atmos. Sci*., **35**, 1712 (1978).

9. A. B. DAVIS, *Radiation Transport in Scale-Invariant Optical Media*, PhD Dissertation, McGill University, Physics Department (1992).

10. HARSHVARDHAN and J. WEINMAN, "Infrared Radiative Transfer Through a Regular Array of Cuboidal Clouds," *J. Atmos. Sci*., **39**, 431 (1982).

11. Z. QU, "On the Transmission of Ultraviolet Radiation in Horizontally Inhomogeneous Atmospheres: A Three-Dimensional Approach Based on the Delta-Eddington's Approximation," PhD Dissertation, University of Chicago, Department of Geophysical Sciences (1999).

12. Y. GU and K.-N. LIOU, "Radiative Transfer in Inhomogeneous Cirrus Clouds Based on the Diffusion Approximation," *Proc. 10th AMS Conf. Atmospheric Radiation*, Madison, Wisconsin, June 28–July 2, 1999, p. 350, American Society for Metals, Boston, Mass (1999).

13. J. A. WEINMAN and M. MASUTANI, "Radiative Transfer Models of the Appearance of City Lights Obscured by Clouds Observed in Nocturnal Satellite Images," *J. Geophys. Res.*, **92**, 5565 (1987).

14. W. J. KOSHAK, R. J. SOLAKIEWICZ, D. D. PHANORD, and R. J. BLAKESLEE, "Diffusion Model for Lightning Radiative Transfer," *J. Geophys. Res.*, **99**, 14361 (1994).

15. A. B. DAVIS, R. F. CAHALAN, J. D. SPINHIRNE, M. J. MCGILL, and S. P. LOVE, "Off-Beam Lidar: An Emerging Technique in Cloud Remote Sensing Based on Radiative Green-Function Theory in the Diffusion Domain," *Phys. Chem. Earth (B)*, **24**, 757 (1999).

16. S. CHANDRASEKHAR, *Radiative Transfer*, Oxford University Press, Oxford, United Kingdom (1950).

17. D. MIHALAS, *Stellar Atmospheres*, Freeman, San Francisco, California (1979).

18. L. C. HENYEY and J. L. GREENSTEIN, "Diffuse Radiation in the Galaxy," *Astrophys. J.*, **93**, 70 (1941).

19. D. DEIRMENDJIAN, *Electromagnetic Scattering on Spherical Polydispersions*, Elsevier, New York (1969).

20. *Radiative Transfer in Scattering and Absorbing Atmospheres: Standard Computational Procedures*, J. LENOBLE, Ed., A. Deepak, Hampton, Virginia (1985).

21. J. ROSS, *The Radiation Regime and Architecture of Plant Stands*, Junk Publications, The Hague, The Netherlands (1981).

22. K. M. CASE and P. F. ZWEIFEL, *Linear Transport Theory*, Addison-Wesley, Reading, Massachusetts (1967).

23. E. RENSHAW and R. HENDERSON, "The Correlated Random Walk," *J. Appl. Probab.*, **15**, 403 (1981).

24. M. D. KING and HARSHVARDHAN, "Comparative Accuracy of Selected Multiple Scattering Approximations," *J. Atmos. Sci*., **43**, 784 (1986).

25. S. LOVEJOY, A. B. DAVIS, P. GABRIEL, G. L. AUSTIN, and D. SCHERTZER, "Discrete Angle Radiative Transfer—Part 1: Scaling, Similarity, Universality and Diffusion," *J. Geophys. Res.*, **95**, 11699 (1990).

26. G. C. POMRANING, "Diffusion Theory via Asymptotics," *Transp. Theory Stat. Phys.*, **18**, 383 (1989).

27. H. C. VAN DE HULST, *Multiple Light Scattering (Tables, Formulas, and Applications*, Academic Press, San Diego, California (1980).

28. G. L. OLSON and P. KUNASZ, "Short Characteristic Solution of the Non-LTE Line Transfer Problem by Operator Perturbation, 1. The One-Dimensional Planar Slab," *J. Quant. Spectrosc. Radiat. Transfer*, **38**, 325 (1987).

29. P. KUNASZ and L. H. AUER, "Short Characteristic Integration of Radiative-Transfer Problems: Formal Solution in Two-Dimensional Slabs," *J. Quant. Spectrosc. Radiat. Transfer*, **39**, 67 (1988).

30. D. J. DURIAN, "The Diffusion Coefficient Depends on Absorption," *Opt. Lett.*, **23**, 1502 (1998).

31. C. D. LEVERMORE and G. C. POMRANING, "A Flux-Limited Diffusion Theory," *Astrophys. J.*, **248**, 321 (1981).

32. G. C. POMRANING, "Flux-Limiting in Three-Dimensional Stochastic Radiative Transfer," *J. Quant. Spectrosc. Radiat. Transfer*, **54**, 637 (1995).

33. M. BASSANI, F. MARTELLI, G. ZACCANTI, and D. CONTINI, "Independence of the Diffusion Coefficient from Absorption: Experimental and Numerical Evidence," *Opt. Lett.*, **22**, 853 (1997).

34. K. FURUTSU and Y. YAMADA, "Diffusion Approximation for a Dissipative Random Medium and its Applications," *Phys. Rev. E*, **50**, 3634 (1994).

35. R. ARONSON and N. CORNGOLD, "Photon Diffusion Coefficient in an Absorbing Medium," *J. Opt. Soc. Am. A*, **16**, 1066 (1999).

36. J. H. JOSEPH, W. J. WISCOMBE, and J. A. WEINMAN, "The Delta-Eddington Approximation for Radiative Flux Transfer," *J. Atmos. Sci.*, **33**, 2452 (1976).

37. M. D. KING, L. F. RADKE, and P. V. HOBBS, "Determination of the Spectral Absorption of Solar Radiation by Marine Stratocumulus Clouds from Airborne Measurements within Clouds," *J. Atmos. Sci.*, **47**, 894 (1990).

38. A. B. DAVIS, A. MARSHAK, R. F. CAHALAN, and W. J. WISCOMBE, "The LANDSAT Scale-Break in Stratocumulus as a Three-Dimensional Radiative Transfer Effect, Implications for Cloud Remote Sensing," *J. Atmos. Sci.*, **54**, 241 (1997).

39. T. Y. NAKAJIMA and M. D. KING, "Determination of the Optical Thickness and Effective Particle Radius of Clouds from Reflected Solar Radiation Measurements—Part 1: Theory," *J. Atmos. Sci.*, **47**, 1878 (1990).

40. R. E. ALCOUFFE, R.S. BAKER, F. W. BRINKLEY, D. R. MARR, R. D. O'DELL, and W. F. WALTERS, "DANTSYS: A Diffusion Accelerated Neutral Particle Transport Code System," LA-12969-M (UC-705), Los Alamos National Laboratory (issued June 1995, revised March 1997).

41. K. F. EVANS, "The Spherical Harmonics Discrete Ordinates Method for Three-Dimensional Atmospheric Radiative Transfer," *J. Atmos. Sci.*, **55**, 429 (1998).

42. A. S. EDDINGTON, "On the Radiative Equilibrium of Stars," *Mon. Not. Roy. Ast. Soc.*, **77**, 16 (1916).

43. G. A. TITOV, "Radiative Horizontal Transport and Absorption in Stratocumulus Clouds," *J. Atmos. Sci.*, **55**, 2549 (1998).

44. S. A. ACKERMAN and S. K. COX, "Aircraft Observations of the Shortwave Fractional Absorptance of Non-Homogeneous Clouds," *J. Appl. Meteor.*, **20**, 1510 (1981).

45. A. MARSHAK, A. B. DAVIS, W. J. WISCOMBE, and R. F. CAHALAN, "Inhomogeneity Effects on Cloud Shortwave Absorption Measurements: Two-Aircraft Simulations," *J. Geophys. Res.*, **102**, 16619 (1997).

46. W. E. MEADOR and W. R. WEAVER, "Two-Stream Approximations to Radiative Transfer in Planetary Atmospheres: A Unified Description of Existing Methods and a New Improvement," *J. Atmos. Sci.*, **37**, 630 (1980).

47. A. SCHUSTER, "Radiation Through a Foggy Atmosphere," *Astrophys. J.*, **21**, 1 (1905).

48. R. F. CAHALAN, W. RIDGWAY, W. J. WISCOMBE, T. L. BELL, and J. B. SNIDER, "The Albedo of Fractal Stratocumulus Clouds," *J. Atmos. Sci.*, **51**, 2434 (1994).

49. H. W. BARKER, "A Parameterization for Computing Grid-Averaged Solar Fluxes for Inhomogeneous Marine Boundary Layer Clouds—Part 1: Methodology and Homogeneous Biases," *J. Atmos. Sci.*, **53**, 2289 (1996).

50. J. L. W. V. JENSEN, "Sur les Fonctions Convexes et les Inégalités entre les Valeurs Moyennes," *Acta Math.*, **30**, 789 (1906).

51. R. F. CAHALAN, W. RIDGWAY, W. J. WISCOMBE, S. GOLMER, and HARSHVARDHAN, "Independent Pixel and Monte Carlo Estimates of Stratocumulus Albedo," *J. Atmos. Sci.*, **51**, 3776 (1994).

52. M. TIEDKE, "An Extension of Cloud-Radiation Parameterization in the ECMWF Model: The Representation of Subgrid-Scale Variations in Optical Depth," *Mon. Wea. Rev.*, **124**, 745 (1996).

53. C. J. CANNON, "Line Transfer in Two Dimensions," *Astrophys. J.*, **161**, 255 (1970).

54. G. L. STEPHENS, "Radiative Transfer Through Arbitrarily Shaped Media—Part 2: Group Theory and Closures," *J. Atmos. Sci.*, **45**, 1836 (1988).

55. G. L. STEPHENS, "Radiative Transfer Through Arbitrarily Shaped Media—Part 1: A General Method of Solution," *J. Atmos. Sci.*, **45**, 1818 (1988).

56. *Dynamics of Fluids in Hierarchical Porous Media*, J. H. CUSHMAN, Ed., Academic Press, San Diego, California (1990).

57. A. MARSHAK, A. B. DAVIS, W. J. WISCOMBE, and R. F. CAHALAN, "Radiative Smoothing in Fractal Clouds," *J. Geophys. Res.*, **100**, 26247 (1995).

58. K. F. EVANS, "A General Solution for Stochastic Radiative Transfer," *Geophys. Res. Lett.*, **20**, 2075 (1993).

59. T. VÁRNAI, "Influence of Three-Dimensional Radiative Effects on the Spatial Distribution of Shortwave Cloud Reflection," *J. Atmos. Sci.*, **57**, 216 (2000).

60. O. A. AVASTE and G. M. VAINIKKO, "Solar Radiation Transfer in Broken Clouds," *Izv. Acad. Sci. USSR Atmos. Oceanic Phys.*, **10**, 1054 (1974).

61. G. A. TITOV, "Statistical Description of Radiation Transfer in Clouds," *J. Atmos. Sci.*, **47**, 24 (1990).

62. F. MALVAGI, R. N. BYRNE, G. C. POMRANING, and R. C. J. SOMERVILLE, "Stochastic Radiative Transfer in a Partially Cloudy Atmosphere," *J. Atmos. Sci.*, **50**, 2146 (1993).

63. B. J. SU and G. C. POMRANING, "A Stochastic Description of a Broken Cloud Field," *J. Atmos. Sci.*, **51**, 1969 (1994).

64. G. MARCHUK, G. MIKHAILOV, M. NAZARALIEV, R. DARBINJAN, B. KARGIN, and B. ELEPOV, *The Monte Carlo Methods in Atmospheric Optics*, Springer-Verlag, New York (1980).

65. L. M. ROMANOVA, "Radiative Transfer in a Horizontally Inhomogeneous Scattering Medium," *Izv. Acad. Sci. USSR Atmos. Oceanic Phys.*, **11**, 509 (1975).

66. G. L. STEPHENS, "Radiative Transfer in Spatially Heterogeneous, Two-Dimensional Anisotropically Scattering Media," *J. Quant. Spectrosc. Radiat. Transfer*, **36**, 51 (1986).

67. A. B. DAVIS, "Physical Thickness and Optical Depth of Stratocumulus from Space-Borne Lidar, A Moment-Based Diffusion Method," *Technical Digest of OSA Top. Mtg. Optical Remote Sensing of the Atmosphere*, Santa Barbara, California, June 21–25, 1999, p. 66, Optical Society of America (1999).

68. L. REYNOLDS, C. JOHNSON, and A. ISHIMARU, "Diffuse Reflectance from a Finite Blood Medium: Applications to the Modeling of Fiber Optic Catheters," *Appl. Opt.*, **15**, 2059 (1976).

69. S. PLATNICK, "A Superposition Technique for Deriving Photon Scattering Statistitics in Plane-Parallel Cloudy Atmospheres," *J. Quant. Spectrosc. Radiat. Transfer*, **68**, 57 (2000).

70. S. PLATNICK, "Approximations for Horizontal Photon Transport in Cloud Remote Sensing Problems," *J. Quant. Spectrosc. Radiat. Transfer*, **68**, 75 (2000).

71. P. M. GABRIEL and K. F. EVANS, "Simple Radiative-Transfer Methods for Calculating Domain-Averaged Solar Fluxes in Inhomogeneous Clouds," *J. Atmos. Sci.*, **53**, 858 (1996).

72. L. CHAMBERS, B. WIELICKI, and K. F. EVANS, "On the Accuracy of the Independent Pixel Approximation for Satellite Estimates of Oceanic Boundary Layer Cloud Optical Depth," *J. Geophys. Res.*, **102**, 1779 (1997).

73. R. F. CAHALAN and J. B. SNIDER, "Marine Stratocumulus Structure During FIRE," *Remote Sens. Environ.*, **28**, 95 (1989).

74. R. F. CAHALAN, "Bounded Cascade Clouds: Albedo and Effective Thickness," *Nonlinear Processes Geophys.*, **1**, 156 (1994).

75. B. B. MANDELBROT, *The Fractal Geometry of Nature*, W. H. Freeman, San Fransisco, California (1982).

76. A. MARSHAK, A. B. DAVIS, R. F. CAHALAN, and W. J. WISCOMBE, "Nonlocal Independent Pixel Approximation: Direct and Inverse Problems," *IEEE Trans. Geosci. Remote Sens.*, **36**, 192 (1998).

77. C. VON SAVIGNY, O. FUNK, U. PLATT, and K. PFEILSTICKER, "Radiative Smoothing in Zenith-Scattered Skylight Transmitted Through Clouds to the Ground," *Geophys. Res. Lett.*, **26**, 2949 (1999).

78. A. B. DAVIS, A. MARSHAK, E. KASSIANOV, and G. M. STOKES, "Three-Dimensional Radiative Transfer Makes its Mark!" *Eos (AGU Trans.)*, **80**, 622 (1999).

79. A. YODH and B. CHANCE, "Spectroscopy/Imaging with Diffusing Light," *Phys. Today*, **48**, 34 (1995).

80. A. B. DAVIS and A. MARSHAK, "Lévy Kinetics in Slab Geometry: Scaling of Transmission Probability," *Fractal Frontiers*, p. 63, M. M. NOVAK and T. G. DEWEY, Eds., World Scientific, Singapore (1997).

81. K. PFEILSTICKER, "First Geometrical Pathlength Distribution Measurements of Skylight Using the Oxygen A-band Absorption Technique—Part 2: Derivation of the Lévy-Index for Skylight Transmitted by Mid-Latitude Clouds," *J. Geophys. Res.*, **104**, 4101 (1999).

82. G. C. POMRANING, *Linear Kinetic Theory and Particle Transport in Stochastic Mixtures*, World Scientific, Singapore (1991).

83. A. B. DAVIS, A. MARSHAK, R. F. CAHALAN, and W. J. WISCOMBE, "Insight into Three-Dimensional Radiation Transport Processes from Diffusion Theory, with Applications to the Atmosphere," *Radiative Transfer—II*, p. 111, M. P. MENGÜÇ, Ed., Begell House, New York (1998).